

THESIS FOR THE DEGREE OF DOCTOR OF PHILOSOPHY

Advanced Materials for Rechargeable Lithium Batteries

JAE-KWANG KIM



Department of Applied Physics

CHALMERS UNIVERSITY OF TECHNOLOGY

Göteborg, Sweden 2013

Advanced Materials for Rechargeable Lithium Batteries

JAE-KWANG KIM

© JAE-KWANG KIM, 2013

Doktorsavhandlingar vid Chalmers Tekniska Högskola

ISBN 978-91-7385-792-5

Ny serie nr 3473

ISSN 0346-718X

Department of Applied Physics

Chalmers University of Technology

SE-412 96 Göteborg

Sweden

Telephone: +46 (0) 31 772 1000

Cover:

**The structure and electrochemical mechanism of
2,3,6,7,10,11-hexamethoxytriphenylene (HMTP) and
poly(2,2,6,6-tetramethylpiperidinyloxy-4-yl methacrylate) (PTMA)
organic electrodes.**

Chalmers Reproservice

Göteborg, Sweden 2013

Advanced Materials for Rechargeable Lithium Batteries

JAE-KWANG KIM

Department of Applied Physics

Chalmers University of Technology

Abstract

Lithium rechargeable batteries have gained much attention in the pursuit for alternative energy sources because of advantages such as high energy density and high electric potential. In addition, the development of low-cost materials has been of interest to reduce the cost of batteries, especially those destined for transportation applications such as electric (EVs) or hybrid-electric vehicles (HEVs). At the same time, safety is a growing concern together with increasing environmental requirements. Moreover, research on light and flexible batteries has also been intensive, motivated by their potential applications in minute electronic systems.

The development of new materials is a key to meet the challenges faced by battery technology. An ionic liquid-based polymer electrolyte could reduce the risk of explosion with non-flammability and high thermal stability. The use of LiMPO_4 cathodes (M=Fe, Mn, Co...) contributes with high thermal stability as a result of the covalent bond between metal and oxygen. Organic electrodes provide flexibility and may facilitate recycling of rechargeable lithium batteries. In this study, these materials have been employed for ultra-safe, flexible, green and high-rate-capability lithium batteries. Raman, XPS, DSC, and dielectric spectroscopy were used to investigate their physical properties, and the electrochemical performance of the ionic liquid-based polymer electrolytes are explored in combination with some LiMPO_4 cathodes. The ion coordination, ionic conductivity, oxidation stability, dissolution of electrode material, and electrochemical properties were investigated. A new nano-fibrous organic radical polymer [(poly(2,2,6,6-tetramethylpiperidinyloxy-4-yl methacrylate) (PTMA)] electrode, a new organic cathode material 2,3,6,7,10,11-hexamethoxytriphenylene (HMTP) containing methoxy functional group (CH_3O) and $\text{Py}_{14}\text{TFSI}$ -based polymer electrolyte to overcome the drawback of organic electrode materials such as high amount of carbon and dissolution of active materials has also been investigated.

Keywords: Rechargeable lithium battery, Ionic liquid-based polymer electrolyte, Organic electrode, rate capability, electrochemical stability, cycle stability.

List of Appended Papers

This thesis is based on the following papers:

I. An imidazolium based Ionic Liquid Electrolyte for Lithium Batteries

J.-K. Kim, A. Matic, J.-H. Ahn, P. Jacobsson, *Journal of Power Sources* 195 (2010) 7639.

II. Highly Porous LiMnPO₄ in Combination with an Ionic Liquid-based Polymer Gel Electrolyte for Lithium Batteries

J.-K. Kim, C.-R. Shin, A. Matic, J.-H. Ahn, P. Jacobsson, *Electrochemistry Communications* 13 (2011) 1105.

III. Towards Flexible Secondary Lithium Batteries: Polypyrrole-LiFePO₄ Thin Electrodes with Polymer Electrolytes

J.-K. Kim, J. Manuel, M.-H Lee, J. Scheers, D.-H. Lim, P. Johansson, J.-H. Ahn, A. Matic, P. Jacobsson, *Journal of Materials Chemistry*. 22 (2012) 15045.

IV. 2,3,6,7,10,11-hexamethoxytriphenylene (HMTP) New Organic Cathode Material for Lithium Batteries

J.-K. Kim, F. Thébault, M.-Y. Heo, D.-S. Kim, Ö. Hansson, L. Öhrström, J.-H. Ahn, P. Johansson, A. Matic, P. Jacobsson, *Electrochemistry Communications* 21 (2012) 50.

V. Nano-Fibrous Polymer Film for Organic Rechargeable Battery

J.-K. Kim, J. Scheers, A. Matic, P. Johansson, J.-H. Ahn, P. Jacobsson, *Journal of Materials Chemistry A* 1 (2013) 2426.

VI. Improving the Stability of an Organic Battery with an Ionic Liquid-based Polymer Electrolyte

J.-K. Kim, A. Matic, J.-H. Ahn, P. Jacobsson, *RSC Advances* 2 (2012) 9795.

Additional papers not included in the thesis

- I. Properties of N-butyl-N-methyl-pyrrolidinium Bis(trifluoromethanesulfonyl) Imide Based Electrolytes as a Function of Lithium Bis(trifluoromethanesulfonyl) Imide Doping
J.-K. Kim, D.-H. Lim, J. Scheers, J. Pitawala, S. Wilken, P. Johansson, J.-H. Ahn, A. Matic, P. Jacobsson, *Journal of the Korean Electrochemical Society* 14 (2011) 92.

- II. Preparation and application of TEMPO-based di-radical organic electrode with ionic liquid-based polymer electrolyte
J.-K. Kim, A. Matic, J.-H. Ahn, P. Jacobsson, C.-E. Song, *RSC Advances* 2 (2012) 10394.

- III. Characterization of N-butyl-N-methyl-pyrrolidinium bis(trifluoromethanesulfonyl)imide-based polymer electrolytes for high safety lithium batteries
J.-K. Kim, L. Niedzicki, J. Scheers, C.-R. Shin, D.-H. Lim, W. Wieczorek, P. Johansson, J.-H. Ahn, A. Matic, P. Jacobsson, *Journal of Power Sources* 224 (2013) 93.

CONTRIBUTION REPORT

I (J.-K. Kim) suggested all projects and refined all projects after discussion.

J.-K. Kim performed all of the experiments and prepared the electrode materials. However, HMTP of paper iv was synthesized by F. Thébault.

J.-K. Kim was the main author of all papers; all writing was done as an iterative process together with the co-authors.

Table of Contents

1 Introduction	1
2 Lithium Rechargeable Battery	3
2.1 Introduction -----	3
2.2 Cathode -----	5
2.3 Anode -----	8
2.4 Membrane and Electrolyte -----	9
3 Materials	13
3.1 Electrospun P(VdF-HFP) membrane -----	13
3.2 Lithium metal phosphate (LiMPO ₄) -----	15
3.3 Organic electrode materials -----	16
4 Experimental	19
4.1 Raman spectroscopy -----	19
4.1.1 Origin of Raman Scattering -----	19
4.1.2 Molecular Vibrations -----	21
4.2 Differential Scanning Calorimetry -----	23
4.3 Coin Cell Assembly -----	25
4.4 Electrochemical Characterization -----	26
4.5 Dielectric Spectroscopy -----	31

5 Summery of Appended Papers	33
6 Conclusions and outlook	35
Acknowledgements	37
Bibliography	38

CHAPTER 1

Introduction

A shift towards sustainable energy is one of the key challenges modern society faces, and an important part of our development of science and technology. The performance of sustainable energy technologies (for example fuel cells, batteries, electrolysis, solar, wind, and supercapacitors) need to be improved to enable better use of intermittent renewable electricity sources. Also, since the climate is changing through global warming via carbon dioxide emissions [1], it is essential to invest in renewable sources of energy for electricity generation and transport. The awareness of both aims relies on developing energy storage installation that balances intermittent supply with consumer demand. However, the development of energy storage also has to assure the safety of human life.

Among the energy conversion and storage systems, rechargeable batteries are attracting attention since they can be used many hundred times. This is in contrast to the primary battery, which is disposed after the energy is consumed. Lead-acid, nickel cadmium (NiCd), nickel metal hydride (NiMH), lithium ion (Li-ion), redox flow, and Na/S are all rechargeable batteries and are, with the exception of the redox flow and Na/S batteries, commonly used in electronic devices. Also, the leaden accumulator, the nickel-cadmium, and nickel metal hydride batteries are used in large storage capacity applications such as UPS (uninterruptible power supply), HEV (Hybrid Electric Vehicle), and stationary storage [2,3].

Among the commercial battery systems the rechargeable lithium battery stands out with excellent properties and is commonly used in portable devices that require low volume and weight, such as laptop computers and mobile phones. The demand for miniature sized secondary batteries has more than doubled between 1995 and 2006, from 180 million to 380 million units sold. Moreover, the market share of lithium rechargeable batteries grew from 47% in 2006 to 70% in 2010 [4]. In addition, the lithium rechargeable battery is a promising power source for hybrid electric vehicles (HEVs) and electric vehicles (EVs) due to the high power and high energy densities [5]. The EV is a good solution to limit CO₂ exhaust and to tackle the limited resource of fossil fuels. After Toyota opened the HEV market in 1997, the market has moved to Plug-in Hybrid Electric Vehicle (PHEV) and to some extent to EV. Much effort has been spent to develop large size lithium batteries that satisfy requirements for mileage, fast charging time, low cost, and high safety. Indeed, novel electrode and electrolyte materials are developed, and considered for commercial lithium batteries.

Poly(ethylene oxide) (PEO) polymer electrolytes have been investigated for application in high safety lithium batteries since they were first reported in 1973 by Fenton *et al* [6]. The ion transfer in PEO occurs through complexation between the polymer and alkali metal salts, which enable its use as a solid polymer electrolyte

(SPE) for electrochemical systems, such as batteries, solar cells, capacitors, and sensors [6,7]. The SPE has many advantages, such as high safety, high flexibility, and high density. However, the ionic conductivity is poor due to low ions mobility. Especially low ionic conductivity at low temperature is a problem, which brings difficulty to commercialization. Additionally, in PEO-based SPEs the mobility of lithium ions decreases with increasing molecular weight [6,7]. To solve the problem of PEO-based electrolytes, branched polymers, crosslinked polymers, block copolymers, and incorporation of ceramic fillers into the PEO matrix have been studied. Also, gel polymer electrolytes, prepared by incorporating organic liquid electrolytes in a porous membrane of a host polymer, have been suggested to improve electrochemical properties, since they possess high ionic conductivity and sufficient mechanical integrity for handling [8-11]. The latter systems are commercially well established today although the liquid electrolyte solvents are volatile and thermally unstable and thus cause safety problems in batteries. As a result, there has been much interest in recent years to replace organic solvents with room-temperature ionic liquids (RTILs), which are non-volatile, non-flammable molten salts with low melting points. RTILs generally exhibit high ionic conductivity, high thermal and chemical stability, a wide electrochemical window, and low toxicity [12,13].

Another goal of lithium rechargeable battery development is mechanical flexibility demanded for weight sensitive applications and various forms of soft, portable electronic devices. To convert such potentials into reality, one paramount challenge is the ability of making flexible electrodes with robust mechanical property and excellent electrochemical performance. Also, such batteries should fit to the life cycles of the applications and should be disposable or recyclable. For the flexible lithium battery, organic conducting materials such as 2,2,6,6-tetramethyl-1-piperidinyloxy (TEMPO)-based polymers, sulfide-based polymer, and carbonyl-based polymers have been used [14-19]. However, the implementation of conducting polymers usually leads to cells with low capacity, self-discharge, poor cycleability, and low rate capability [14,20]. Also, the organic materials are subjected to low potential, dissolution into liquid electrolytes, low thermal stability, and need a high amount of carbon conductor material.

In my thesis, RTILs are incorporated in a nano-fiber polymer matrix for the preparation of polymer gel electrolytes. The ionic liquid-based polymer electrolytes are investigated in terms of ionic conductivity, thermal behavior, molecular structure, and oxidation stability. As a final test, the ionic liquid based-polymer electrolytes are applied to lithium rechargeable batteries with a lithium metal phosphate cathodes and organic cathodes for ultra safe lithium batteries. Also, novel framework cathodes such as polypyrrole composited LiFePO_4 , 2,3,6,7,10,11-hexamethoxytriphenylene (HMTP) and nano-fibrous PTMA were studied with the aim to improve properties and stability of flexible rechargeable batteries.

CHAPTER 2

Lithium rechargeable battery

2.1 Introduction

One of the most viable candidates as a sustainable energy conversion and storage systems is the rechargeable lithium ion battery (LIB), which was commercialized by Sony in the early 1990s. The LIB has the last two decades witnessed a dramatic growth in sales (close to 10 billion dollars in 2009) [1,2]. The LIB is based on a cathode and an anode, which has the property of reversible insertion and extraction of lithium ions. Transfer of lithium ions is enabled by the addition of an organic liquid electrolyte and a mechanical separator between the anode (negative electrode) and the cathode (positive electrode). When the lithium ion is inserted and extracted in the cathode and the anode, electrical energy is generated by electrochemical oxidation and reduction (Figure 2.1).

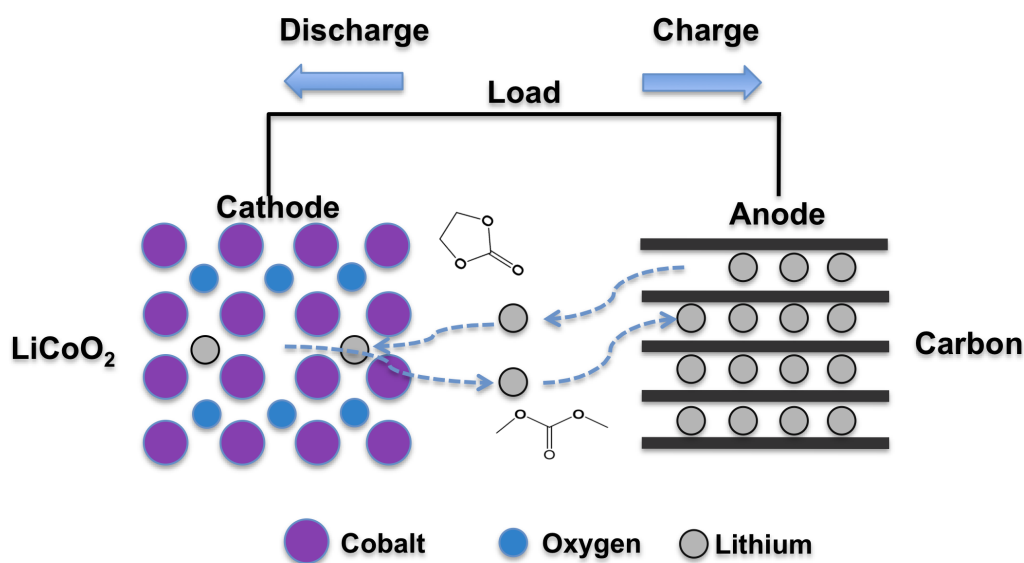


Figure 2.1: Principle of a rechargeable lithium ion battery.

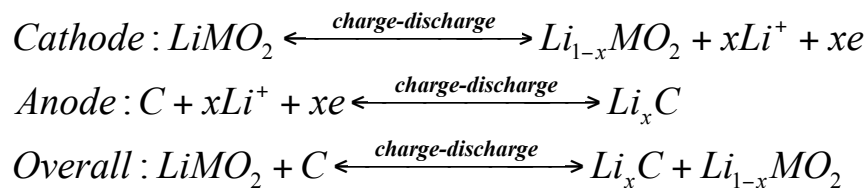
In the commercial LIBs lithium is introduced as lithiated carbon (i.e. as LiC_6) in the anode, although there is hope to in the future utilize pure lithium metal anodes for ultimate power density. Carbon as anode material marked the turnaround for the lithium ion rechargeable battery in the early 1990's because it prevented the dendrite formation, which short-circuit the battery when a lithium metal anode is used. Thus, the carbon anode was a revolution for safe lithium ion insertion/extraction. Actually, this anode material has high reversibility and a reaction potential close to the oxidation/reduction of lithium metal, resulting in a high energy density. It is also considered environment-friendly and economically efficient.

On the cathode side transition metal oxides (LiMO_2), such as LiCoO_2 , act as electron and Li-ion acceptors during the discharge process. However, the cathode material has to be replaced by cheaper and more environmentally friendly materials for electric vehicle (EV) applications. Many compounds such as transition metal oxides, sulfides, and organic materials (polymers) have been proposed as replacements. Oxide and sulfide materials have been studied due to high theoretical capacity. However, the sulfide cathode is dependent on the use of a lithium metal anode because the sulfide has no lithium ions in the structure and oxide cathodes, such as LiCoO_2 , LiNiO_2 , $\text{LiNi}_{1-x}\text{Co}_x\text{O}_2$, LiMnO_2 , LiMn_2O_4 , and $\text{LiCo}_x\text{Ni}_y\text{Mn}_{1-x-y}\text{O}_2$, have low thermal stability [21]. More recently LiFePO_4 has attracted much attention and even introduced on the commercial market, as a cathode material to replace LiMO_2 , due to high cycle stability, low cost and high thermal stability [22]. Polymer based cathodes are also studied for flexible lithium batteries [23].

The electrolyte between the anode and cathode has to be an ionic conductor, electronic insulator and is responsible for the transport of lithium ions. The optimal electrolyte should combine the conduction properties of a liquid and the mechanical stability of a solid with high chemical stability. Even though liquid electrolytes are commonly used, due to high ionic conductivity, application of polymer and ionic liquid electrolytes are also attracting interest since they might improve the safety of lithium batteries [13].

A membrane (separator) is an important component of a battery, as it prevents short circuit by separating the anode from the cathode. In the LIB, the membrane is required to be capable of battery shutdown at a temperature below that at which thermal runaway occurs, and the shutdown should not result in loss of mechanical integrity. Otherwise, the electrodes could come into direct contact and the resulting chemical reactions cause thermal runaway. Shutdown is an important trait of a good membrane for the safety of lithium batteries. The promising membranes are those with high electrolyte permeability and mechanical strength, as well as good thermal, chemical, and electrochemical stability.

The electrochemical reactions at the typical LIB cell are:



Each component (the anode, the cathode, the electrolyte and the membrane) has to be compatible with each other to provide high safety, cycle ability, high capacity, and high rate capability [24]. The LIB is highly interesting for application in EV with improved safety as the main concern. At the same time, much effort to overcome the 250 Wh/kg limitations of lithium batteries is in progress, by development of new type of batteries.

2.2 Cathode

Since 1980 when the LiCoO_2 , with a 274 mAh/g theoretical capacity, was first demonstrated as a possible cathode material for rechargeable lithium ion batteries, the transition metal intercalation oxides have caught the major attention as cathode materials. The conventional cathode materials belong to layered compounds LiMO_2 (M=Co, Ni, Mn, etc.), spinel compounds LiM_2O_4 (M=Mn, Fe, etc.), and olivine compound LiMPO_4 (M=Fe, Co, Mn, etc.). The layered structure of LiMO_2 is shown in Figure 2.2. The oxygen anions form a close-packed *fcc* lattice with cations located in the six coordinated octahedral crystal site. The MO_2 slabs and Li layers are stacked alternatively [25]. The spinel structure of LiM_2O_4 is displayed in Figure 2.3. The oxygen site of LiM_2O_4 is the same as in the LiMO_2 layered structure. The cations (M) occupy the octahedral site but $1/4$ of them are located in the Li layer, leaving $1/4$ of the sites in transition metal layer vacant. Li ions occupy the tetrahedral sites in Li layer that share faces with the empty octahedral sites in the transition metal layer. The structure is based on a three-dimensional MO_2 host and the vacancies in transition metal layer ensure three-dimensional Li diffusion pathways [25]. The Olivine structure of LiMPO_4 will be described in detail in the materials section (Chapter 3).

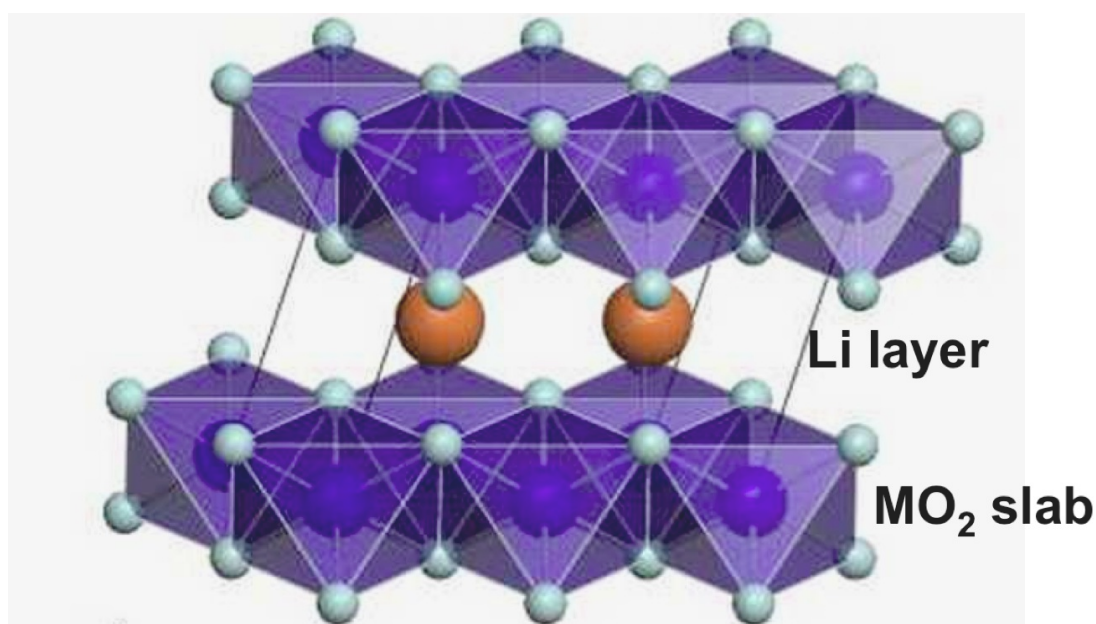


Figure 2. 2: Crystal structure of layered LiMO_2 (blue: transition metal, gold: Li ions) (Courtesy of Prof. Nakayama).

Cathode materials for LIB are designed to optimize two important factors, energy density and cyclability. The energy density is determined by the reversible capacity and operating voltage, which are mostly determined by the materials intrinsic chemistry, such as the effective redox couples and maximum lithium ion concentration in the active material. For cycling performances, electronic and ionic mobility are key determining factors, though particle morphologies are also important factors due to the anisotropic nature of the structures.

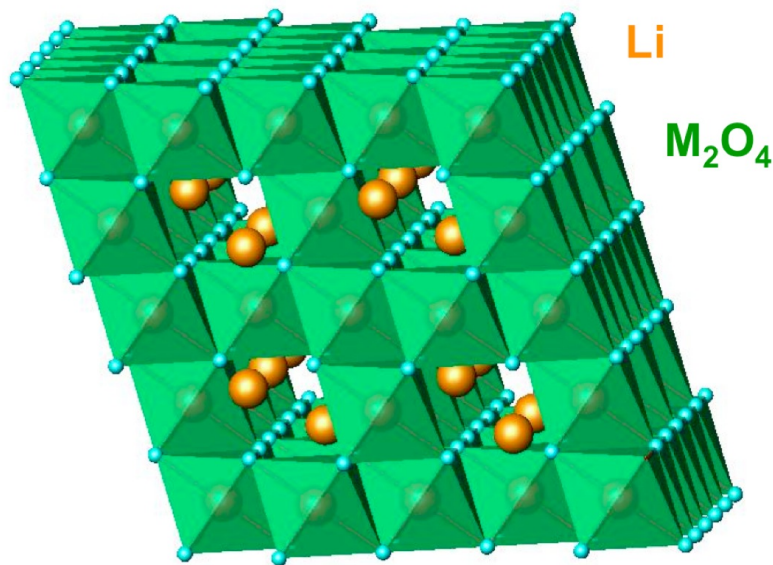


Figure 2. 3: Crystal structure of spinel LiM_2O_4 (green: transition metal ions, gold: Li ions) (Courtesy of Prof. Petkov).

LiCoO_2 is still used in most lithium batteries designed for portable devices due to the high energy density and the good cycle performance. However, Co is relatively expensive and toxic. Therefore, application of nickel (Ni) and manganese (Mn), which are elements of low cost and abundant deposits, is increasing instead of Co. Although LiNiO_2 has a larger practical capacity compared to LiCoO_2 (180 vs 140 mAh/g), the cell potential is lower and the thermal stability is worse. LiMn_2O_4 (120 mAh/g practical capacity) is a safer alternative with good overcharge characteristic but has a drawback, the dissolution of manganese and destruction of crystal structure at high temperature. Also, composites of nickel and cobalt with LiMn_2O_4 are studied. For example $\text{LiNi}_{1/3}\text{Co}_{1/3}\text{Mn}_{1/3}\text{O}_2$ (170 mAh/g practical capacity) is more and more used for application in electronic devices. Outside of that, $\text{LiFe}_x\text{Ni}_y\text{Mn}_{1-x-y}\text{O}_2$ is studied for good safety, long cycling life and low price. Nevertheless, the metal oxide electrode materials are still potentially dangerous because they provide oxygen that might be released and induce a battery explosion at harsh conditions [21]. So, the development of new cathode materials is crucial.

Around 1997, Armand et al. and Goodenough et al. independently found that lithium metal phosphate (LiMPO_4) has a very stable structure [26,27], due to covalent bonding between oxygen and phosphor, and LiFePO_4 was developed as a response to economic and environmental concerns. LiFePO_4 offers several advantages, such as a theoretical specific capacity of 170 mAh/g and a high flat voltage versus charge characteristic at 3.4 V vs lithium. The latter provides a wider safety margin for use with organic electrolytes, good reversibility of the cathode reactions, high thermal and chemical stability, low material costs, low toxicity, and stable cycling performance [23,27]. Co and Mn might substitute Fe in LiFePO_4 to give LiMnPO_4 and LiCoPO_4 with increased energy densities. However, LiMnPO_4 has a problem of dissolution of

Mn into organic liquid electrolytes and LiCoPO_4 has a very low electrical conductivity [25-29].

	LiCoO_2	LiNiO_2	LiMn_2O_4	$\text{Li}[\text{Ni}_{1/3}\text{Co}_{1/3}\text{Mn}_{1/3}]\text{O}_2$	$\text{Li}[\text{Ni}_{1/2}\text{Mn}_{1/2}]\text{O}_2$	LiFePO_4
Theoretical capacity	274 mAh/g	275 mAh/g	148 mAh/g	285 mAh/g	285 mAh/g	170 mAh/g
Available Capacity	145 mAh/g	185 mAh/g	120 mAh/g	170 mAh/g	170 mAh/g	150 mAh/g
Voltage	3.7 V	3.6 V	3.8 V	3.7 V	3.7 V	3.45V
Advantage	High conductivity Easy synthesis	- High capacity - Stability of electrolyte	- Low price - Non-toxic	- High capacity - Low price - Good thermal stability	- High capacity - Low price - Good thermal stability	- Low Price - Environmental friendly
Disadvantage	- High cost - Toxic	Difficult synthesis and fabrication of thin film - Thermal instability	- Low capacity - Capacity fading @ High Temp	Low tap density compared to LiCoO_2	Low conductivity ($<10^{-8}$ S/cm)	Low Conductivity ($<10^{-9}$ S/cm)

Table 2.1: Properties of cathode materials for rechargeable lithium batteries [25].

Inorganic cathode materials are synthesized using a number of techniques such as solid-state, sol-gel, mechanical activation, hydrothermal, co-precipitation, spray, microwave, and supercritical method. The synthesis conditions are very important for the final properties of the cathode material. Therefore, the synthesis parameters have been optimized by numerous groups to enhance the electrochemical performance [22].

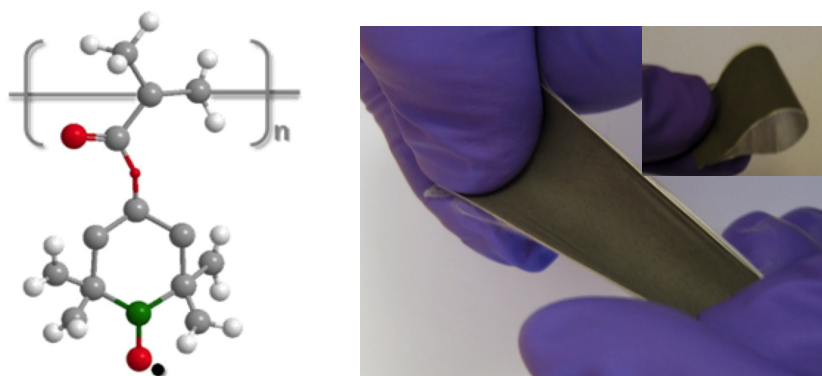


Figure 2. 4: Structure of PTMA (left) and a flexible electrode based on the PTMA polymer (right).

For flexible electronic devices, there is a high demand for thin and flexible batteries, driven by their potential application in micro- and nano-electronic systems. To meet this demand, many attempts have been made to synthesize novel active electrode materials. For this purpose cathodes based on organic/polymeric materials are more advantageous, compared to the conventional cathode materials based on transition metal oxides, since the former are light, environment-friendly and easily

processed to thin films with good flexibility. The polyaniline (PAni), polypyrrole (PPy), and organic radical PTMA (poly(2,2,6,6-tetramethylpiperidinyloxy-4-yl methacrylate)) have both gained much attention as active cathode materials for flexible batteries (see figure 2.4)[23,30,31].

2.3 Anode

The active anode material occupies 10 weight percent of lithium rechargeable battery and releases electrons during the oxidation stage. In the early attempts, pure lithium was directly used as anode in lithium metal batteries, but it was later substituted by lithiated carbon because of safety problems due to dendrite formation. Important properties of an anode material are potentials near to the electrode potential of lithium, high energy densities per volume and weight, safety during charge-discharge processes, perseverance of high current densities, and high thermal stabilities [32].

Carbon materials for anodes can be divided into hard and soft carbon. The hard carbon is obtained from resin and pitch, and the soft carbon is natural and artificial graphite. In addition to the carbon type, the carbon properties depend on the preparation temperature [33]. Graphite has the most satisfying anode properties and has been widely used in commercial lithium batteries.

	Li metal	Graphite	Si ($\text{Li}_{22}\text{Si}_5$)	Sn ($\text{Li}_{22}\text{Sn}_5$)	SnO, SnO ₂ , Al, Pb, Ge, Nano-Co, Nano-Ni
Characteristics	High energy density	Low theoretic capacity (372 mAh/g)	High theoretic capacity (4200 mAh/g)	High theoretic capacity (990 mAh/g)	Capacity (2200~500 mAh/g)
	High activity	Low cost	Large volume expansion (320 %)	Large volume expansion (670 %)	Large volume expansion
	Not proper to thin film battery	Low irreversible capacity	Large irreversible capacity Poor cycleability	Large irreversible capacity Poor cycleability	Large irreversible capacity Poor cycleability

Table 2. 2: Properties of anode materials for lithium rechargeable batteries [33,34].

Si, Sn, Ge, Al, and Sb are also studied as anode materials for lithium batteries. They form alloys with lithium and attract much attention because the theoretical capacity of the alloyed anode materials are higher than the graphite anode ($\text{Li}_{4.4}\text{Si}$: 4200 mAh/g, $\text{Li}_{4.4}\text{Ge}$: 1600 mAh/g, $\text{Li}_{4.4}\text{Sn}$: 990 mAh/g, and Li_3Sb : 660 mAh/g). Another advantage of the alloyed anode is the possibility of using propylene carbonate-based electrolytes (PC) that destroy the frame of graphite carbon, and

safety via a higher reaction potential [34]. Despite the advantages, the alloyed anode has found limited applications because they undergo large volume changes upon insertion and extraction of lithium ions. The large volume change induces cracks in the electrode and leads to an abrupt capacity fade [34].

2.4 Membrane and Electrolyte

The membrane (separator) is a porous film between the anode and the cathode that prevents an electrical short. Polyethylene (PE) and polypropylene (PP) belong to the class of polyolefin's and are the most common membrane materials for rechargeable lithium batteries [4]. Porous polyolefin membranes are suitable for batteries, since they can be used for hundreds of cycles without any chemical or physical degradation. A collapse of the pores occurs when the temperature approaches the melting point (around 130 °C) of the material, which then forms a nonporous insulated film and results in a sharp increase in impedance. Since the impedance of a PP separator increases less than that of a PE separator, the impedance of the PP membrane may not be large enough for complete shutdown, and thermal runaway could still happen. Therefore, porous PE is the preferred membrane material for most LIBs. The polyolefin membranes can be prepared by two different processes; a dry method or a wet method. In the dry method a PP/PE/PP triple layer pore structure of cylindrical form is formed. The wet method results in a single layer PE with a wood-like pore structure [35-37].

parameter	Unit	goal
Conductivity	(S/cm)	>10 ⁻⁴
Thickness	(µm)	<25
Electrical resistance	(Ohms cm ²)	<2
Pore size	(µm)	<1
Porosity	(%)	~40
Puncture strength	(kg/s ²)	>1x10 ⁸
Mix penetration strength	(kg/s ²)	>4x10 ⁷
Tensile strength	(%)	<2% offset at 1000 psi
Shutdown temp.	(°C)	~130
High-temp. melt integrity	(°C)	>150
Chemical stability		stable in battery for long period of time
Dimensional stability		separator should lay flat; be stable in electrolyte

Table 2. 3: Required properties of membranes swollen with an electrolyte for rechargeable lithium batteries [35-39].

The main disadvantages of polyolefin membranes are poor thermal stability at high temperatures and danger of internal short, due to the weak mechanical strength, leading to thermal runaway – even explosions in the extreme case. Therefore, ceramic-based membranes are investigated to resolve the disadvantages associated with polyolefin membranes [35]. The ceramic membranes are prepared with inorganic

sub-micron sized particles and a small amount of polymer binder, which have dimensional stability at a high temperature as well as wettability. Ceramic membranes that improve the thermal and mechanical stability, are also made by ceramic coating of felt and hybrid form polyolefin [38,39]. This type of separator is highly desirable for the development of large-size lithium batteries, especially those installed in electric vehicles and power tools. The membrane should usually meet the following requirements summarized in Table 2.3 [35-39].

The electrolyte provides a pathway for ion transfer between the cathode and anode. It should have a high ionic conductivity, good compatibility with the electrode materials and should not react with lithium ions. The electrolyte is usually a liquid where a lithium salt is dissolved in an organic solvent [40]. Aqueous electrolytes are not possible to use in rechargeable lithium batteries because the aqueous electrolyte is decomposed at a voltage of 4.2 V. Thereby, organic solvents are usually applied in lithium batteries.

Currently, commercial lithium battery electrolytes use organic carbonate based solvents, such as propylene carbonate (PC) and ethylene carbonate (EC), and LiPF_6 , LiBF_4 , and LiAsF_6 as lithium salts. The use of these electrolytes allows the realization of high performance batteries. However, since the solvents are flammable, their use poses serious safety risks and strongly reduces the batteries operational temperature range [41]. For this reason, alternative electrolytes have been proposed and studied. Among the alternative electrolytes, ionic liquid-based electrolyte and polymer electrolytes appear to be the most promising.

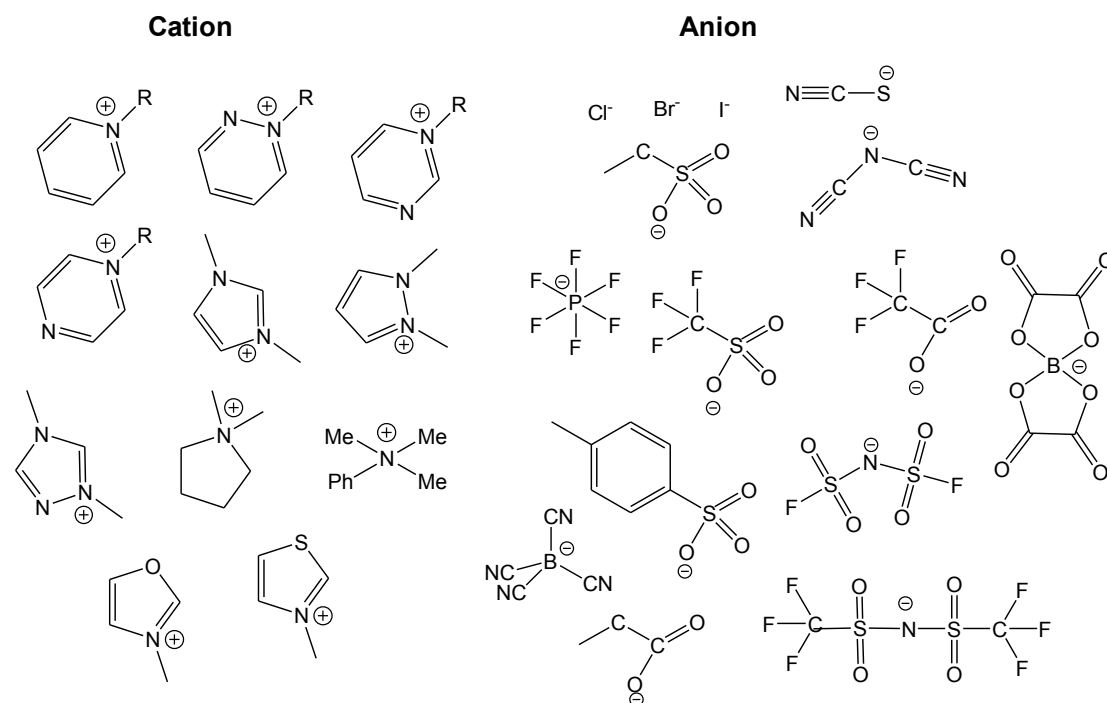


Figure 2. 5: Structure of anions and cations for ionic liquids.

Ionic liquids are molten salts, composed only of ions (Figure 2.5). Room temperature ionic liquids (RTILs) are molten salts having a melting point below room

temperature. The cation, for example based on imidazolium, pyrrolidinium, piperidinium, phosphonium or pyridinium, can be modified by incorporation of side groups on the ring. With a large number of possible anions, for example $[\text{BF}_4]^-$, $[\text{PF}_6]^-$, $[\text{N}(\text{CN})_2]^-$, $[\text{C}_4\text{F}_9\text{SO}_3]^-$, $[\text{CF}_3\text{CO}_2]^-$, $[\text{CF}_3\text{SO}_3]^-$, $[\text{N}(\text{CF}_3\text{SO}_2)_2]^-$, $[\text{N}(\text{FSO}_2)_2]^-$ and $[\text{CF}_3\text{CONCF}_3\text{SO}_2]^-$ the properties of RTILs can be tailored through the selection of cation and anion. Several attempts have been made to tailor new RTILs intended as solvents for lithium salts; some examples are N-alkyl-N-methylmorpholinium bis(trifluoromethylsulfonyl) imide, Triethyl(methoxymethyl) phosphonium bis(trifluoromethylsulfonyl) amide and Trialkylsulfonium dicyanamides [19,20,41,42]. However, so far the ionic conductivity obtained has been lower than expected due to increasing viscosity with the addition of salt and a high degree of ion-ion interactions [43].

The solid polymer electrolyte is another alternative electrolyte suggested decades ago in order to improve the safety of rechargeable lithium batteries [13]. The solid polymer electrolyte is prepared with a lithium salt dissolved in a polar polymer. The poly(ethylene oxide) (PEO) based electrolyte is still one of the most promising and widely studied solid polymer electrolytes because of its good mechanical and thermal properties, and interfacial stability towards lithium metal. Here the archetypal polymer electrolyte is PEO-LiX, prepared by blending PEO with a suitable lithium salt (LiX, where X denotes a charge delocalized anion). The transport of lithium ions within the solid electrolyte has been associated with the local relaxation and segmental motion of the amorphous regions in the PEO chains [13,42]. These polymers often show high crystallinity at low temperatures and the electrolytes thus exhibit low ionic conductivity at room temperature (typically $\leq 10^{-5}$ S/cm). This drawback of the solid polymer electrolytes necessitates operation at high temperatures (generally, >70 °C) for successful utilization in practical applications. With PEO-based gel electrolytes, formed by incorporating molecular solvents that can compete with the ether oxygen atoms “O” of the polymer for coordinating the lithium ion, significantly higher ionic conductivities have been reported at room temperature. However, the reactivity of the solvents, which leads to poor interfacial stability with lithium metal, and their volatile nature causes safety concerns and unexpected short circuits in the battery [13,14,44-46].

Gel polymer electrolytes (GPEs) have attracted much attention since they show high ionic conductivities at room temperature [16]. GPEs are made by immobilizing large amounts of liquid electrolyte in a polymer host. Porous polymer hosts have been developed to fit GPEs. In porous polymer electrolytes, the polymer host is a membrane with pores of nanometer to micrometer size that retain the liquid electrolyte [16-18]. The membrane should have the capability to absorb the liquid electrolyte without leakage, be chemically compatible with electrode materials, and adhere well to the electrodes. Poly(vinylidene fluoride) (PVdF), poly(vinylidene fluoride-co-hexafluoropropylene) {P(VdF-HFP)}, polyacrylonitrile (PAN), PEO, and poly(methyl methacrylate) (PMMA) have been widely studied as host polymers for preparing GPEs (Figure 2.6). PVdF and its copolymer P(VdF-HFP), are particularly preferred as polymer hosts for GPEs because of their thermal and electrochemical stability. The porous membranes are prepared by different methods that include solution casting, phase inversion, plasticizer extraction, and electrospinning [18,47-49]. The size and distribution of the pores are important factors that determine the

membrane's ability for electrolyte uptake. The process of electrospinning is particularly suitable for producing thin and homogenous polymer membranes with pores in the nano- to micrometer size range. Since the membranes possess high porosity, they also exhibit a high electrolyte uptake that results in an ionic conductivity almost in par with the neat electrolyte [18,49].

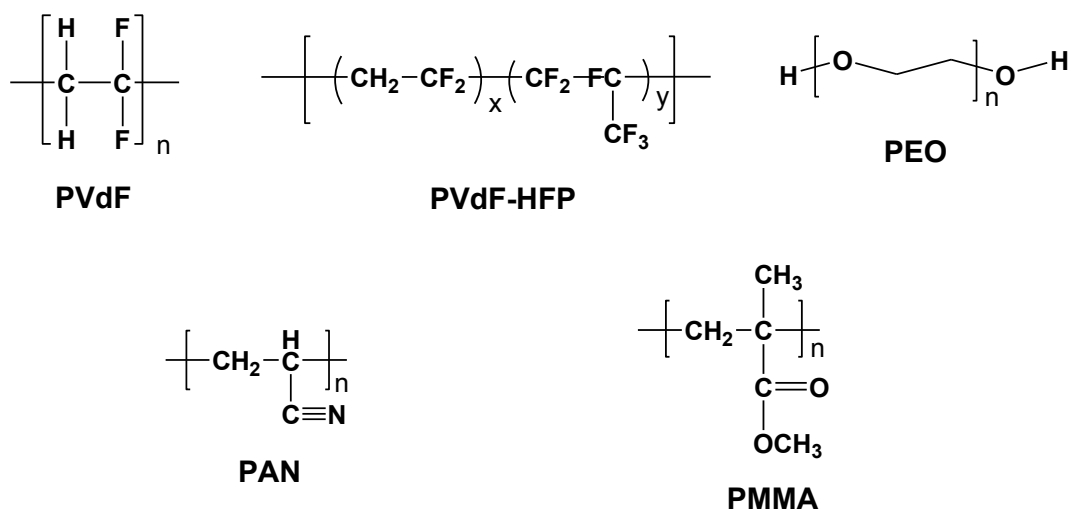


Figure 2. 6: Structures of host polymers for gel polymer electrolytes.

Conventional GPEs have properties in between liquid and polymer electrolytes. They still have poor non-flammability and poor behavior at low temperature. On the other hand, ionic liquid-based GPEs have the advantages of both ionic liquids and polymer electrolytes for high ionic conductivity and high safety. However, the latter suffer from a low lithium transference number, as a result of the strong ion-ion interaction. Several research groups have suggested adding an organic solvent additive to improve the lithium transference number of these systems, and they also report that the incorporation of ceramic fillers such as SiO_2 , TiO_2 and Al_2O_3 is able to increase the ionic conductivity and reduce the ion coordination [50-55].

CHAPTER 3

Materials

3.1 Electrospun P(VdF-HFP) membrane

Electrospinning is techniques where fibers with a diameter on the nm to μm scale are spun together, using an electric field, to form a porous membrane. There is virtually no limit on the selection of materials to be used, compared to previously known self-assembly, phase separation, and template synthesis method. Furthermore, high specific surface area and porosity are attainable by electrospinning, which has attracted a lot of attention [56-58]. The electrospinning device consists of a syringe pump that can push a viscous liquid precursor, a DC high voltage power supply, a needle for extracting nano-fibers, and a substrate connected to ground (see figure 3.1 for a schematic). The basic principle of operation relies on that continuous fibers are elongated under high electric fields and form on the grounded bottom substrate. The requirement on the polymer solution or melt is a sufficient degree of viscosity, approximately of the order 1 to 200 poise [56]. When the electric field is applied to the polymer solution, hanging in the form of a droplet at the end of the vertically located capillary in equilibrium between gravity and surface tension, a charge or dipole repulsion is induced at the air/droplet interface, generating a force that oppose the surface tension. As a result, the surface of the droplet is elongated into a conical shape known as the Taylor Cone; the jet of the charged polymer solution is emitted from the end of the cone when the repulsive electrostatic force overcomes the surface tension at threshold electric field strengths [57]. In low viscosity solutions, the surface tension disrupts the jet into fine droplets. However, with increasing viscosity, the jet does not collapse, but fly through the air towards the collector plate while the solvent evaporates, and the charged, continuous phase polymer fiber accumulates on the collector plate. While flying toward the collector plate, the trajectory of the jet bends or changes direction. In addition, as the jet becomes thinner during the flight, and the charges are collected on the surface, the initial single jet is divided into several smaller filaments – known as splaying. The main process variables in electrospinning are: the solution characteristics (concentration, viscosity, and surface tension), the distance between the end of the capillary tube to the collector plate, the electric field strength, radiation time, and radiation environment. The form of fibers depends on these process variables. If the distance from the end of the capillary to the collector plate is too short, solvent containing fibers reach the collector plate and adhesion between fibers occur during drying. Since this effect is similar to the heat or solvent bonding of non-woven fabrics, the interlayer adhesion between fibers and layers is strengthened in the web made by electrospinning. In addition, when the intensity of the electric field is increased, the total charge density of the jet is increased and thinner fibers are obtained. Nano-fibers in the form of beads are the result of the collapse of the jet under the electric field modified by surface tension. The major factors formatting nano-fibers in the form of beads are the solution viscosity, total charge density of jets, and the surface tension of the solution. High viscosity polymer solutions make fibers without beads. The distance between beads increases and the

beads get bigger as the viscosity increase, but the shape changes from spherical to spindle forms. As the total charge density gets higher, fibers without beads as well as thinner fibers are obtained. Fibers made by electrospinning have a very thin diameter and high specific surface area per unit volume, which cannot be obtained via other existing technologies, and in particular the porous surface of the fiber enables the application of electrospun fibers in a variety of fields [58].

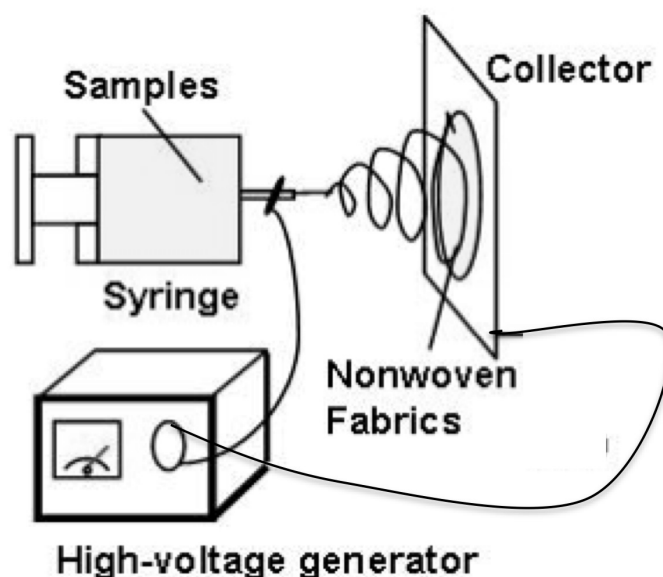


Figure 3.1: Scheme of the electrospinning process

Two types of pores exist in fibers made by electrospinning: pores inside or on the surface fiber; and pores due to the gap between the fibers. When compared to mesoporous materials such as molecular sieves, electrospun fibers have small specific surface area but pores, which are interconnected in three-dimensional network structure, are relatively large in size. The pore size and porosity is important variables in determining the performance of the membrane: porosity indicates the extent to flow across the membrane, whereas the pore size determines the degree for a particular substance sweeps through the membrane.

The P(VdF-HFP) co-polymer (Kynar Flex 2801, $M_w = 4.77 \times 10^5$, VdF/HFP ratio: 88/12, Elf Atochem) was vacuum dried at 60 °C before use. The solvents, acetone and *N,N*-dimethylacetamide (DMAc) (HPLC grades, Aldrich), were used as received. P(VdF-HFP) solutions of varying concentration (12–18 wt.%) were prepared in a mixed solvent of acetone/DMAc (in varying proportions, 3:7, 5:5 and 7:3, w/w) by mechanical stirring for 30 min at room temperature. The polymer solution was fed through a capillary using a syringe pump (KD Scientific, Model 210) and a high electric voltage (varied between 11 and 24 kV) was applied to the capillary by means of a power supply. A thin aluminum foil fixed on a grounded; stainless-steel current collector in the shape of a drum rotating at a specified speed was used to collect the charged polymer in the form of a membrane. The electrospun membrane was vacuum dried at 60 °C for 12 h before further use [18,49].

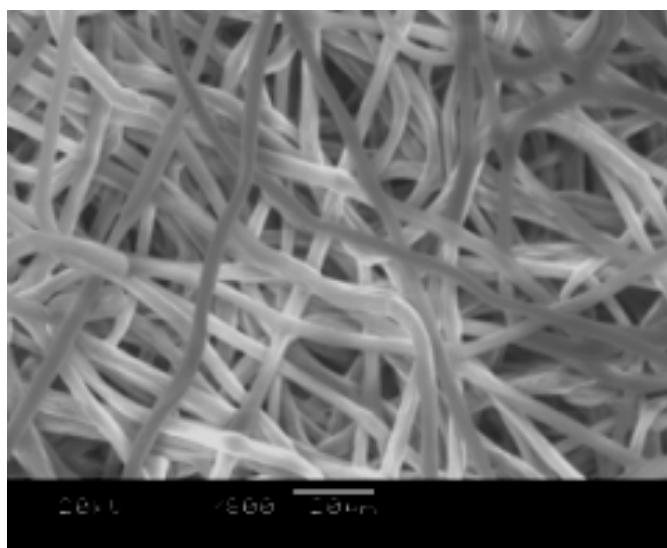


Figure 3. 2: P(VdF-HFP) fibrous membrane prepared by electrospinning.

3.2 Lithium metal phosphate (LiMPO₄)

Lithium metal phosphate (LiMPO₄, M=Co, Fe, Mn...) is an olivine; MNXO₄ [Figure 3.3], where M and N are cations with different sizes. Olivine is the hexagonal analog of spinel, containing a slightly distorted *hcp* anion array with half of the octahedral sites and one edge of octahedral occupied by cations. In olivine, two types of octahedral sites are energetically distinguishable, possibly leading to an ordering of different cations between them (ordered olivine), as in LiMPO₄. The structure is composed of PO₄ tetrahedra and MO₆ octahedra, as shown in Figure 3.3. Thus, Li atoms occupy chains of edge-shared octahedra running parallel to the *c*-axis, in alternate *a-c* planes, while the M atoms occupy zig-zag chains of corner-shared octahedra running parallel to the *c*-axis in the other *a-c* planes [59]. The *a-c* planes containing the Li atoms are bridged by PO₄ tetrahedra.

Goodenough and co-workers presented LiFePO₄ as the most promising candidate for low cost cathode because it is abundantly available, environmentally benign, has a large theoretical capacity of 170 mAh/g, and also exhibits excellent thermal stability in the fully charged state [60]. However, LiFePO₄ requires further additional processing to overcome the limitations of poor electronic conductivity ($\sim 10^{-9}$ Scm⁻¹) [61] and slow lithium ion diffusion [62]. Solutions to this end, such as coating LiFePO₄ particles with conductive materials, for example carbon [63-71] or metal [72], dispersing metal particles [73], and solid-solution doping by cations have been proposed [63,74].

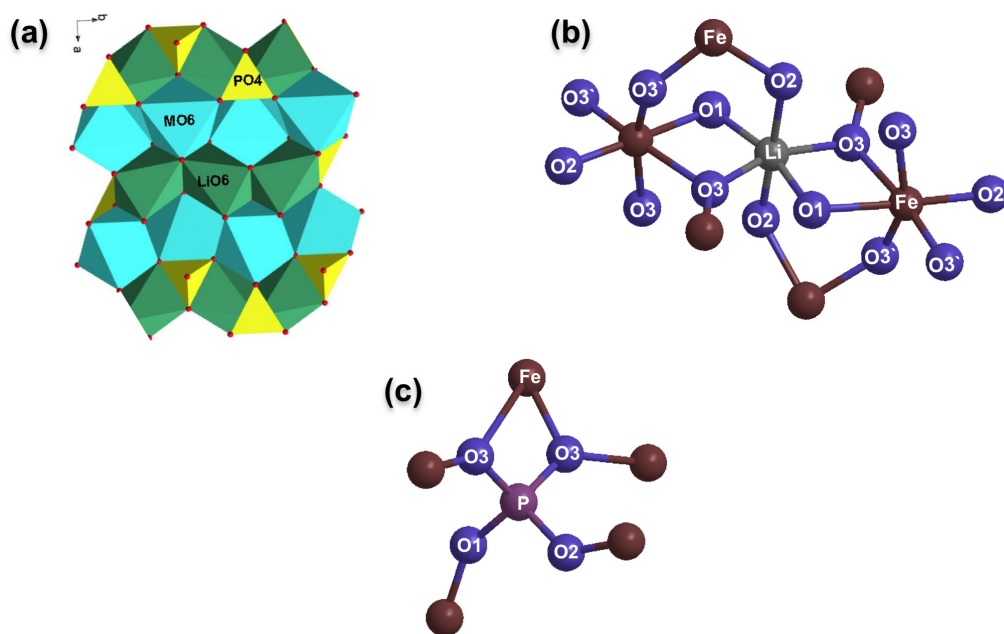


Figure 3. 3: (a) The structure of LiFePO₄. The P atoms occupy tetrahedral 4c sites (light shading) and the Fe atoms occupy octahedral 4c sites (dark shading). The light shaded circles represent the Li ions. The oxygen atoms are arranged in a hexagonal closed-packed arrangement. (b) A view of the close neighbors of the Li ion where the small dark spheres represent the oxygen atoms and the big dark spheres represent the Fe atoms. (c) A view of the close neighbors of the P atom where the small dark spheres represent the oxygen atom and the big dark spheres represent the Fe atoms.

Among other lithium metal phosphates, LiMnPO₄ and LiCoPO₄ attract attention due to their high operation potential (Mn=4.4V, Co=4.9V). However, they both have a drawback that must be solved: Mn dissolution into the electrolyte from LiMnPO₄ and decomposition of electrolyte at the operation potential of LiCoPO₄.

3.3 Organic electrode materials

Poly(2,2,6,6-tetramethylpiperidinyloxy-4-yl methacrylate) (PTMA) has the nitroxide radical 2,2,6,6-tetramethyl-1-piperidinyloxy (TEMPO) as its repeating unit. The active repeating radical unit of the polymer has a low molecular weight of 156 and the unpaired electron is almost fully localized in the radical. TEMPO possesses good chemical stability because of resonance structures and steric protection of the radical center [75]. TEMPO and its polymer exhibit reversible oxidation-reduction behavior in aprotic solvents [76,77]. It is well established that nitroxide radicals like TEMPO undergo rapid redox reactions with an electron-transfer rate constant of the order of 10⁻¹ cm/s [78], which is several orders higher as compared to that of the organic redox couples like disulfides (~10⁻⁸ cm/s at room temperature) [79]. On oxidation of the nitroxide radical, a p-type doping occurs in a reversible manner and an oxoammonium cation is formed. PTMA was synthesized by the radical polymerization method. The synthesis steps followed are shown in Figure 3.4. 2,2,6,6-tetramethylpiperidine methacrylate monomer was polymerized by first using

2,2'-azobisisobutyronitrile radical initiator and then oxidizing with H₂O₂ in the presence of NaWO₄ catalyst to obtain PTMA.

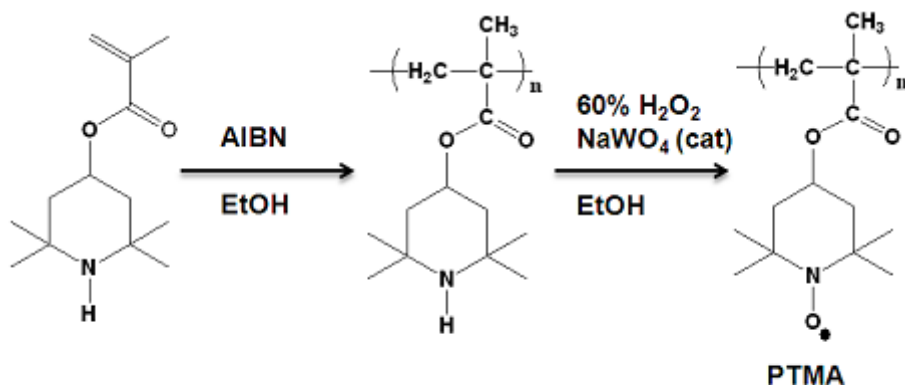


Figure 3. 4: Synthesis process of PTMA.

Figure 3.5 shows the electrochemical mechanism of PTMA with an ionic liquid electrolyte {N-butyl-N-methyl-pyrrolidiniumbis(trifluoromethanesulfonyl)imide (Py₁₄TFSI) and lithium bis(trifluoromethanesulfonyl)imide (LiTFSI)}. The nitroxyl radical of TEMPO is oxidized to form a cation and combines with an electrolyte anion (TFSI⁻) to form oxoammonium salt during the anodic stage and the reverse reaction occurs during the cathodic stage. The existence of such a redox couple of radical makes PTMA an attractive cathode-active material for use in lithium batteries. However, since PTMA is an insulator large amounts, generally around 40 wt.%, of conductive fillers, like carbon black, are used in the electrodes, substantially limiting the effective cathode capacity.

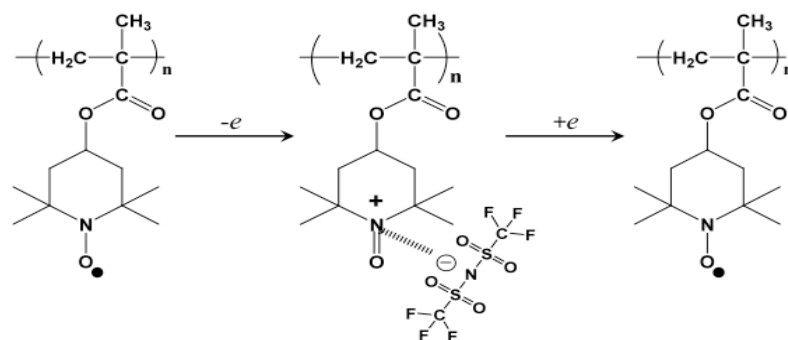


Figure 3. 5: Electrochemical mechanism of PTMA with TFSI⁻ anion.

For practical applications, it is essential to increase the active material content of the cathode. Moreover, PTMA show high self-discharge due to the dissolution into conventional/organic electrolytes.

2,3,6,7,10,11-hexamethoxytriphenylene (HMTP) show similar reduction-oxidation potentials as compared to PTMA, and high rate capability and stable cycling. Each molecular unit contains six methoxy functional groups (CH₃O)

substituted onto a central triphenylene group (Figure 3.6). The bulk material agrees as hexagonal with space group $P6_3/m$ from the single crystal structure [80].

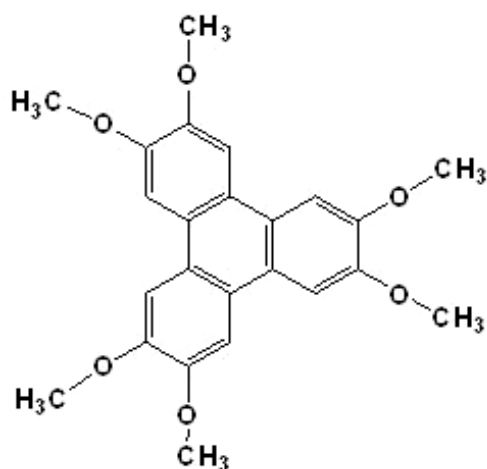


Figure 3. 6: Molecular structure of 2,3,6,7,10,11-hexamethoxytriphenylene (HMTP).

For synthesis of HMTP, A solution of veratrol (13.82 g, 100 mmol) in dichloromethane (140 ml) was added drop-wise to a suspension of $\text{FeCl}_3 \cdot \text{H}_2\text{O}$ in dichloromethane (300 ml) and concentrated sulfuric acid (0.7 ml). After complete addition, the reaction mixture was further stirred for 3 h at room temperature, then methanol was slowly added under vigorous stirring. The mixture was further stirred for 30 minutes and the precipitate was filtered off, washed with methanol and dried under reduced pressure to give a slightly beige powder. The one electron reduction process of HMTP during the discharge leads to the formation of a radical anion; HMTP^\bullet . The delocalization stabilizes the HMTP^\bullet radical and thus leads to a reduced self-discharge.

CHAPTER 4

Experimental

4.1 Raman spectroscopy

Raman scattering (or the Raman effect) is a phenomenon changing the wavelength of scattered light. It was discovered by Raman et al. in 1928 when they observed green light when blue light was sent through a solvent [81-84]. Afterwards, owing to the development of spectrometers measuring the Raman scattering, Raman spectroscopy, using the spectrum that expresses the intensity of the scattered light as bands or series of peaks according to the frequency, has been used to measure the molecular vibrational spectrum. Raman spectroscopy is used to investigate the molecular structure for qualitative and quantitative analysis of substances.

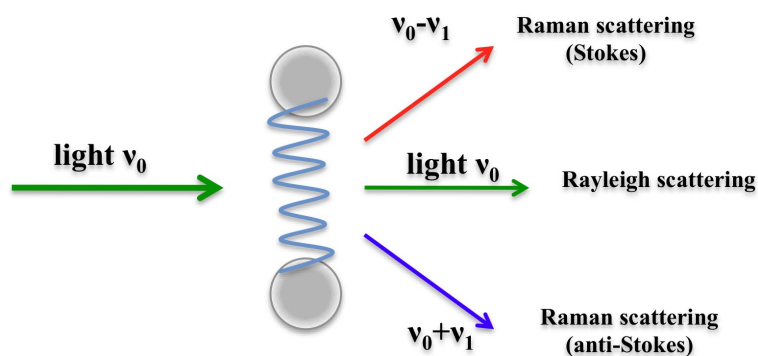


Figure 4. 1. Rayleigh and Raman scattering; frequency of incident light (ν_0) and frequency of molecular vibration (ν_1).

4.1.1 Origin of Raman Scattering

When lights pass through any medium, some of the light scatters and deviates. Most of the scattered light keeps the original energy but some of the photons of the scattered light have less or more energy than original. The scattering process conserving the original energy is called Rayleigh scattering, or elastic scattering. The inelastic scattering process, where energy is lost or gained, is called Raman scattering. When molecules interact with light, they can be excited, and then immediately relax back. If they relax back to the same vibrational level the light will have the same energy (frequency) as the incident light, Rayleigh scattering. If it returns to a higher or lower vibrational level the molecule has absorbed or released vibrational energy ($h\nu_1$), Raman scattering (Figure 4.1). In this case the electronic state remains the same, but a transition of vibrational state has occurred. The process where the system returns to a higher vibrational energy level is called Stokes Raman scattering, ($h\nu_0 - h\nu_1$), and when the system returns to a lower vibrational level the process is called Anti-Stokes Raman scattering, ($h\nu_0 + h\nu_1$), (Figure 4.2), here, ν_0 and ν_1 corresponds to

the wave number of each vibrational mode, and h is Planck's constant [81].

Through the Raman scattering processes, energy exchange between the incident light and the material takes place. Because the absorbed (or released energy) is directly related to the molecular structure of each substance, see further below on Molecular vibrations, the molecular structure of a substance can be deduced by analyzing the Raman scattered light. However, the vibrational energy cannot be measured directly, as in the case of infrared absorption spectroscopy. Instead it is measured by observing and comparing how much energy has been changed compared to the incident light. The amount of shift in frequency of the scattered light from Rayleigh scattering is indicated in the spectrum as the Raman shift, which corresponds to the frequency of vibration of the molecule [82,83]. In general, the number of molecules in the ground state is greater than the number of molecules in excited vibrational states, so Stokes Raman scattering has a larger intensity than the anti-Stokes Raman scattering. Therefore, it is common to measure only the Stokes side in a Raman experiment.

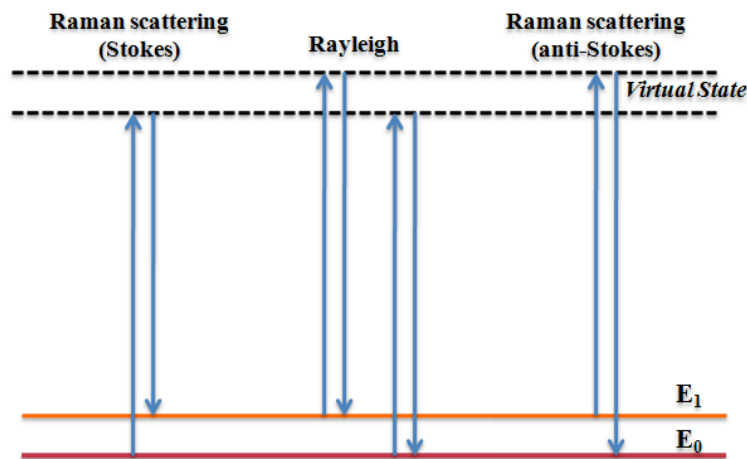


Figure 4. 2: Energy level diagram for Stokes Raman, Rayleigh and anti-Stokes Raman scattering.

The important features of Raman scattering can be explained by a simple classical electromagnetic field description [81]. The dipole moment, μ , induced in a molecule by an external electric field, E , is proportional to the field.

$$\mu = \alpha E \quad (4.1)$$

If during a vibration of a molecule one or more of the components in the polarizability (α) tensor are changed, the vibration is Raman active. The intensity of the scattering can be shown to be proportional to the square of Eq. 4.2.

$$\frac{\partial \alpha}{\partial Q} \neq 0 \quad (4.2)$$

The population of the vibrational states is expressed by the Bose-Einstein occupation factor $n(\omega)$.

$$n(\omega) = \frac{1}{e^{\frac{h\omega}{K_B T}} - 1} \quad (4.3)$$

and the intensities of Stokes and anti-Stokes line can be shown to be

$$I_{stokes} \propto \frac{(\omega_0 - \omega_{vib})^4}{\omega_{vib}} \cdot (n(\omega) + 1) \quad (4.4)$$

and

$$I_{anti-stokes} \propto \frac{(\omega_0 + \omega_{vib})^4}{\omega_{vib}} \cdot n(\omega) \quad (4.5)$$

So, the ratio between Stokes and anti-Stokes line is expressed as [81]

$$\frac{I_{stokes}}{I_{anti-stokes}} = \left(\frac{\omega_0 - \omega_{vib}}{\omega_0 + \omega_{vib}} \right)^4 \cdot e^{\frac{h\omega}{K_B T}} \quad (4.6)$$

4.1.2 Molecular Vibrations

Different chemical groups give different vibrational spectra. A linear molecule such as CO₂ with 3 atoms has $3N-5$ ($N=3$) normal modes of vibration, while a non-linear molecule such as H₂O has $3N-6$ ($N=3$) normal modes of vibration. $3N$ is the number of degrees of freedom of motion.

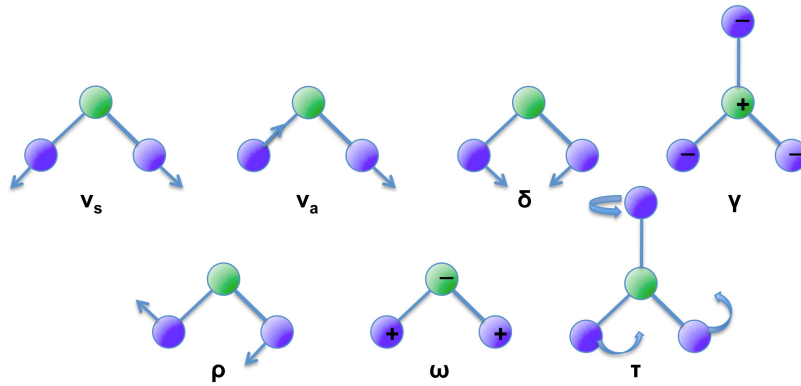


Figure 4. 3: Vibrational modes in a polyatomic molecule: the symmetric and anti-symmetric stretching (v_s and v_{as}), in-plane bending (δ), out of plane bending (γ), rocking (ρ), wagging (ω), and twisting (τ) modes.

The normal vibrations are identified as stretching modes, which mainly change the bond length between atoms (symmetric v_s and anti-symmetric v_{as}): bending modes, which mainly change the angles between atoms (in-plane δ and out-of-plane γ): and finally rocking (ρ), wagging (ω), and twisting (τ) modes, as shown in Figure 4.3.

The vibrational frequencies depend on the masses of the atoms in the molecule, the atomic arrangement, the chemical environment and the chemical bond strengths. Therefore, different molecules have different vibrational spectra [84]. For example,

CO stretching modes are found in the frequency range $1000-1400\text{ cm}^{-1}$ whereas CH modes are found at $2800-3000\text{ cm}^{-1}$ due to the reduced mass. Moreover, OH stretch modes are observed at even higher frequencies in the range of $3200-3700\text{ cm}^{-1}$. For the observation of molecular vibrations, infrared spectra (IR) and Raman spectra are commonly used together in the analysis. (Figure 4.4).

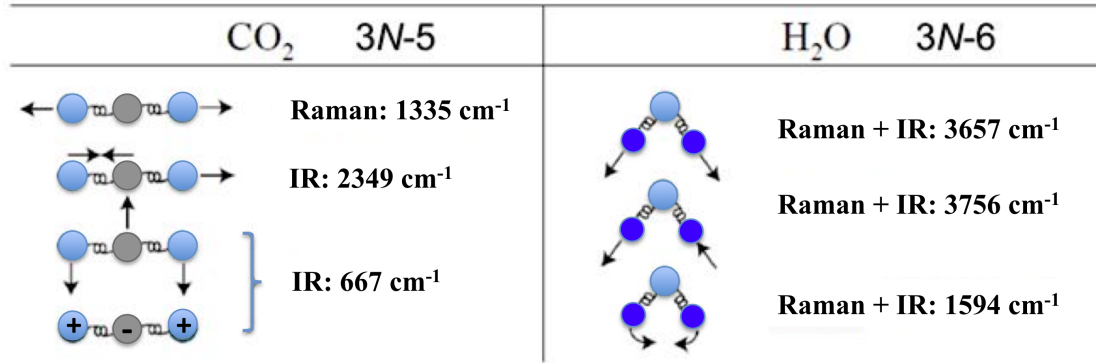


Figure 4. 4: Vibration modes of CO_2 (linear molecule) and H_2O (non-linear molecule).

Consider the vibration of a diatomic molecule in which two atoms of the masses (m_1 and m_2) are connected by a chemical bond. Here, r_1 and r_2 are the distances from the center of gravity. If r_1+r_2 is the equilibrium distance and x_1 and x_2 are the displacements of atoms. Then, the relationships are required with the conservation of the center of gravity:

$$m_1 r_1 = m_2 r_2 \quad (4.7)$$

$$m_1 (r_1 + x_1) = m_2 (r_2 + x_2) \quad (4.8)$$

Combining these two equations, we obtain

$$x_1 = \left(\frac{m_2}{m_1}\right)x_2 \text{ or } x_2 = \left(\frac{m_1}{m_2}\right)x_1 \quad (4.9)$$

In the classical treatment, the chemical bond is regarded as a spring that obeys Hooke's law, where the restoring force, f , is expressed as

$$f = -K(x_1 + x_2) \quad (4.10)$$

Here K is the force constant, and the minus sign indicates that the directions of the force and the displacement are opposite to each other. From (4.9) and (4.10).

$$f = -K\left(\frac{m_1 + m_2}{m_1}\right)x_2 = -K\left(\frac{m_1 + m_2}{m_2}\right)x_1 \quad (4.11)$$

Newton's equation of motion ($f=ma$, m =mass, a =acceleration) is written for each atom as

$$m_1 \frac{d^2 x_1}{dt^2} = -K \left(\frac{m_1 + m_2}{m_2} \right) x_1 \quad (4.12)$$

$$m_2 \frac{d^2 x_2}{dt^2} = -K \left(\frac{m_1 + m_2}{m_1} \right) x_2 \quad (4.13)$$

introducing the reduced mass (μ) and displacement (q), (4.10) is written as

$$\mu \frac{d^2 q}{dt^2} = -Kq \quad (4.14)$$

The solution of this differential equation is

$$q = q_0 \sin(2\pi\nu_0 t + \varphi) \quad (4.15)$$

where q_0 is the maximum displacement and φ is the phase constant, which depend on the initial conditions. ν_0 is the classical vibrational frequency given by

$$\nu_0 = \frac{1}{2\pi} \sqrt{\frac{K}{\mu}} \quad (4.16)$$

In this study, the ion coordination in ionic liquid electrolytes was investigated through Raman scattering.

4.2 Differential Scanning Calorimetry

Differential scanning calorimetry (DSC) is a widely used thermal analysis technique in various research areas. The thermal response of a material, heat effects associated with phase transitions and chemical reactions as a function of temperature are analyzed in DSC. The difference in heat needed to increase the sample temperature, compared with a reference, is measured as a function of temperature [85,86]. The heat flow is related to enthalpy changes and the difference in the heat flow can be written as

$$\Delta \frac{dH}{dt} = \left(\frac{dH}{dt} \right)_{\text{sample}} - \left(\frac{dH}{dt} \right)_{\text{reference}} \quad (4.17)$$

When the heat flow to the sample is higher than to the reference, due to heat absorption, $\Delta dH/dt$ in Eq. 4.17 is positive and the process is called endothermic. Glass transition and melting belong to the class of endothermic processes. In an exothermic process, the heat flow is opposite and $\Delta dH/dt$ is negative. Crystallization, cross-linking, oxidation, and decomposition reactions are all exothermic processes. The

integral of the DSC curve over the region where a particular process occurs, e.g. over a melting peak, gives the total enthalpy change for the process (4.18).

$$\int \left(\frac{dH}{dt}\right)_{\text{sample}} dt = \Delta H_{\text{sample}} \quad (4.18)$$

The glass transition is shown as a discrete change of the baseline, and corresponds to a change in the heat capacity (C_p) of the sample. The heat capacity of the sample can in this case be obtained by comparing the baseline of the sample with that of the reference.

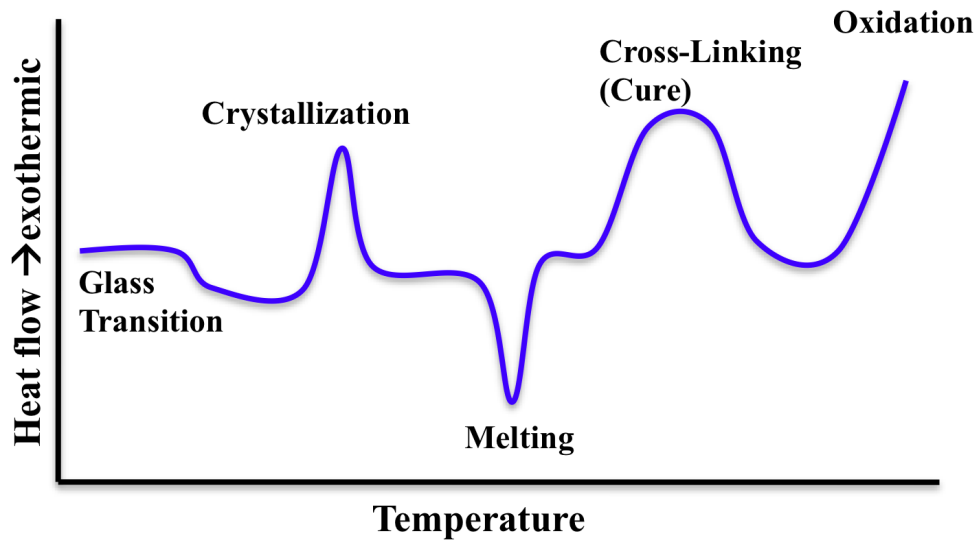


Figure 4.5: Typical DSC thermogram.

The DSC apparatus consists of a sample holder and a reference holder as shown in Figure 4.6. Platinum is commonly used for the holder. A metallic disk separates the sensors used to analyze the heat flow, and keeps the sample and the reference in thermal contact. A resistance heater and a thermocouple are positioned under each holder.

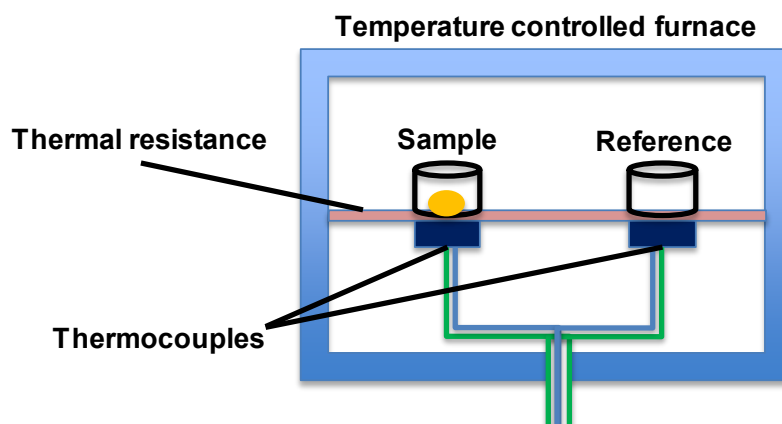


Figure 4. 6: Schematic diagram of the DSC.

The sample and reference have independent heaters. Usually, the reference is an empty aluminum pan and a similar pan is used for the sample. The sample is placed in the pan, located in the holder, which can be heated or cooled at a suitable rate. A flow of nitrogen gas is kept over the sample and the reference to create a reproducible and dry atmosphere. The nitrogen atmosphere also removes air - preventing oxidation of the sample at high temperatures.

4.3 Coin Cell Assembly

Electrochemical investigations of materials for rechargeable lithium batteries are usually performed within cell assembly, where (1) cylindrical, (2) coin (button), (3) Swagelok, and (4) pouch cell are used. The pouch and cylindrical cells dominate industry scale batteries and Swagelok or coin type cells are applied to lab scale batteries where the amount of materials available is limited. In this thesis coin cells were used for most of the electrochemical measurements.



Figure 4.7: Types of rechargeable lithium battery [(1) cylindrical, (2) coin (button), (3) Swagelok, and (4) pouch cells].

Electrode materials (active materials) are mixed with a carbon conductor (carbon black) and a binder (PVdF) in N-methylpyrrolinone (NMP) solvent to prepare electrodes (cathode and anode). The viscous slurry is spread on a substrate (Al or Cu) by the doctor blade method. For electrochemical tests, moisture on the electrodes has to be removed by vacuum drying.



Figure 4.8: Parts of a coin cell [(1) can, (2) anode, (3) gasket, (4) separator, (5) cathode, (6) metal plate, (7) spring, and (8) cap].

The coin cell is composed of (1) can, (2) anode, electrolyte, (3) gasket, (4) separator, (5) cathode, (6) metal plate, (7) spring, and (8) cap. The assembly is performed in argon filled glove box. The vacuum dried anode (lithium metal) is located in the center of the can and the electrolyte is added in proper amount. The separator covers the anode and electrolyte is added to the separator. After the gasket is fixed, the dried cathode is positioned on the same place as the anode. The metal plate covers the cathode to prevent movement of the electrode, next the spring and the coin cell is closed with the cap. The assembled cell is sealed by pressing together the cell.

4.4 Electrochemical Characterization

The electrochemical cell is composed of a working electrode, a counter electrode, and an electrolyte between the electrodes. When the electrolyte contains an electro-active material, Faradic and capacitive currents are generated by a potential that can induce a redox reaction of the electro-active material. The transport of charges between the electrodes and electrolyte has to overcome the polarization resistance (R_p) and the charge transfer resistance (R_{ct}). Electrochemical impedance or AC impedance is the response of an electrochemical cell to an applied potential [87]. The application of an alternating current signal allows investigation of the phase of the AC part of the current, resistance and capacitance of the electrochemical cell [88,89].

In the AC impedance experiment the current flows through a resistor and capacitor (C_d) of a parallel circuit and the total resistance follows Ohm's Law. If the resistances could be expressed as $Z_2(\omega)$ and $Z_3(\omega)$, the complex resistance (Z_1) is given by equation 4.19.

$$\frac{1}{Z_1(\omega)} = \frac{1}{Z_2(\omega)} + \frac{1}{Z_3(\omega)} \quad (4.19)$$

where ω is $2\pi f$ (f is the frequency), Z_2 is R_p and Z_3 is $1/(j\omega C_d)$. So, Eq. 4.19 becomes

$$\frac{1}{Z_1(\omega)} = \frac{1}{R_p} + j\omega C_d \quad (4.20)$$

The total complex resistance (Z) of the electrochemical cell is obtained by the addition of R_s into Eq. 4. 20.

$$Z(\omega) = R_s + Z_1(\omega) = R_s + \frac{R_p}{1 + \omega^2 R_p^2 C_d^2} - \frac{j\omega R_p^2 C_d}{1 + \omega^2 R_p^2 C_d^2} \quad (4.21)$$

The complex resistance is a function of frequency and is composed of a real and an imaginary part. Therefore, the Eq. 4.21 can be rewritten as

$$Z = Z' + jZ'' \quad (4.22)$$

Z' and Z'' have units of ohm and are each expressed as.

$$Z' = R_s + \frac{R_p}{1 + \omega^2 R_p^2 C_d^2}$$

$$Z'' = \frac{-\omega R_p^2 C_d}{1 + \omega^2 R_p^2 C_d^2}$$
(4.23)

AC impedance is very useful practical tool to identify a property of electrode and electrolyte on lithium rechargeable battery. The impedance plot (Nyquist plot) consists of a real impedance (Z') and an imaginary impedance ($-Z''$) part. The plot can also give information about electrolyte resistance, electron transfer resistance, double layer capacitance, and diffusion coefficient from Warburg impedance [90].

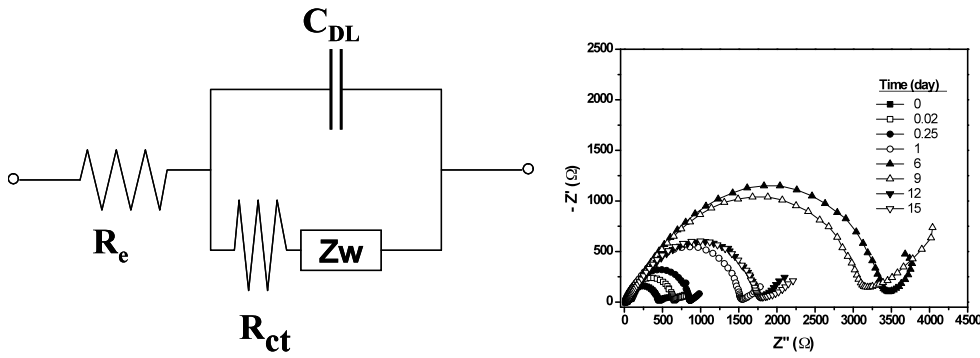


Figure 4.9: Equivalent circuit used for fitting the electrochemical impedance spectroscopy (EIS) data (left) and Impedance behavior (Nyquist plot) of a gel polymer electrolyte (right).

Figure 4.9 shows the simplified equivalent circuit model to analyze the impedance spectra. It contains the constant resistance of the electrolytes (R_e or R_s), charge transfer resistance (R_{ct}), Warburg impedance (Z_w) and double layer capacitance (C_{DL} or C_d). The response of a gel polymer electrolyte generally exhibits a single semi-circle impedance, typical of materials having high ionic conductivity with contributions from resistance of the electrolyte (R_e) in the high frequency range and the charge transfer resistance (R_{ct}) in the middle frequency range. The semi-circle at high frequencies is due to the parallel combination of C_{DL} and R_{ct} , the value obtained by analysis of the high frequency data.

The inclined line at the low frequency (right hand side of figure 4.9) represents the Warburg impedance (Z_w), which is related to lithium ion diffusion in the electrode. The lithium-ion diffusion coefficient (D) in the electrode may be obtained from either the 45° portion of the line or from equation (4.24) and (4.25):

$$D = \frac{R^2 T^2}{2n^4 F^4 C^2 \sigma^2}$$
(4.24)

where R is the gas constant, T is the Kelvin temperature, n is the number of electrons per molecule during oxidization, F is the Faraday constant, C is the concentration of

lithium ion, and σ is the Warburg factor. The Warburg factor σ can be obtained from equation (4.24):

$$Z'' = \sigma\omega^{1/2} \quad (4.25)$$

In a gel polymer electrolyte, the electrolyte resistance is almost constant in time/cycling but the electron resistance decrease and the lithium ion diffusion coefficient increases with cycling because of improved penetration of lithium ions in the electrodes.

Linear sweep voltammetry (LSV) is a general term applied to any voltammetric method in which the potential applied to the working electrode is varied linearly in time. For instance, the oxidation stability of an electrolyte is evaluated by LSV. These methods would include polarography, cyclic voltammetry (CV), and rotating disk voltammetry. The slope of the ramp has units of volts per unit time, and is generally called the scan rate of the experiment. LSV is useful to observe decomposition voltage of electrolytes with low scan rate (<5 mV/s). The decomposition voltage of the ionic liquid-based gel polymer electrolytes was measured by LSV (Figure 4.10).

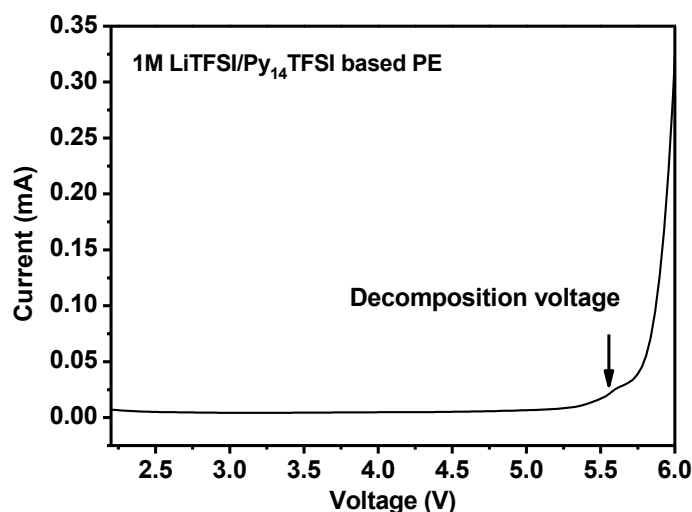


Figure 4.10: Linear sweep voltammetry (LSV) of LiTFSI/Py₁₄TFSI based polymer electrolyte (scan rate: 0.1 mV/s).

Cyclic Voltammetry (CV) measures a change of current generated between a working electrode and a counter electrode according to the applied potential. CV is often the first experiment performed in an electrochemical study to determine the Cut-off voltage for charge-discharge tests. CV typically shows two peaks, one when increasing the potential and one when decreasing the potential (Figure 4.11).

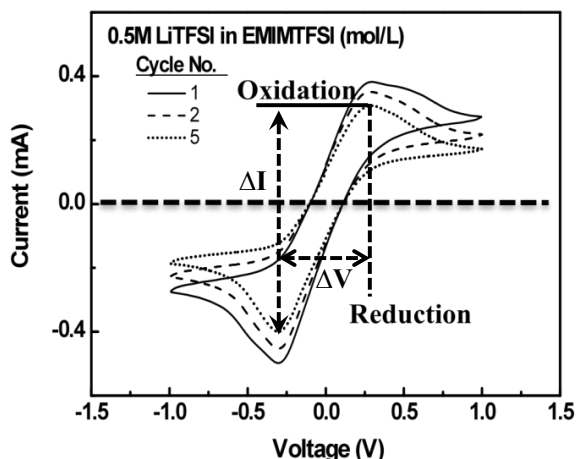


Figure 4. 11: CV curves during cycling of an ionic liquid-based electrolyte Li half cell at 25 °C. (scan rate: 0.1 mV/s)

The positive current peak increases with oxidation of electrode material and decrease again when the oxidation is finished on electrode. The negative current peak increases with reduction of the electrode. The voltage difference (ΔV) between the oxidation and reduction peaks divided with the current (ΔI) is proportional to the cell resistance and the area of each peak shows the amount of transported electrons [89,91]. Thus, we are able to evaluate the reversible reaction and cell resistance through CV.

In this thesis, the evaluation of CV will be illustrated by observation of the one electron reduction of ionic liquid-based gel polymer electrolytes (Figure 4.11). The redox couple exhibits nearly a reversible electrode reaction without any complications of proceeding or undesired chemical reactions.

The performance of a rechargeable lithium battery is estimated by charge-discharge tests. Electrode active materials have their intrinsic potential and capacity, and the evaluation of a charge-discharge test yields these properties. The test starts at the open circuit voltage (OCV), where the cell is not connected to an electric circuit. Since the OCV is changed with self-discharge of the active material, this measurement reveals whether self-discharge exist or not. The OCV depends on the electrode material and resistance between electrolyte and electrode.

The intrinsic capacity theoretical capacity of the active material is calculated by Faraday's Law (Eq. 4.26) [89].

$$\text{Theoretical capacity} = \frac{nF}{3600 \times M} (\text{mAh / g}) \quad (4.26)$$

where n is the number of electrons released/accepted per molecular unit, F is Faraday's constant, and M is the molecular weight.

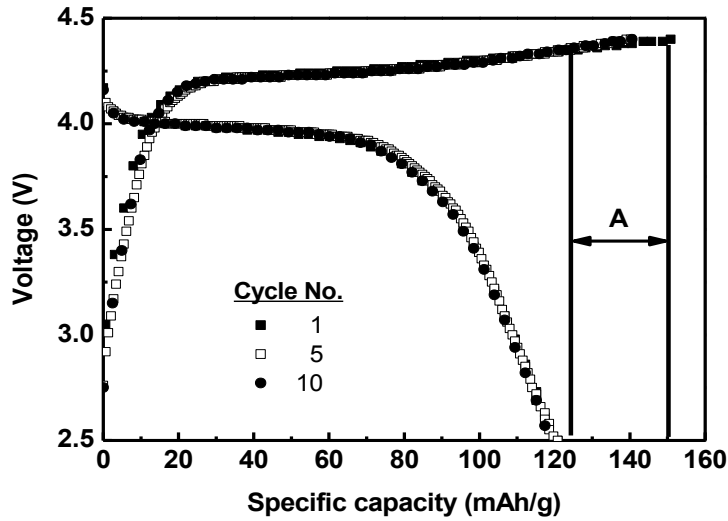


Figure 4.12: Charge-discharge performance of a LiMnPO₄ battery.

From the charge-discharge curve, a reversible reaction between oxidation and reduction, utilization of electrode material, Columbic efficiency, and energy density are usually estimated [92]. For example, a LiMPO₄ cathode with 170 mAh/g theoretical capacity shows 71 % (=121/170) utilization in figure 4.12. The irreversible reaction (A) between charging and discharging is 20 % and the Columbic efficiency of LiMnPO₄ is thus 80 %. LiMnPO₄ has a potential of 4.1V and an energy density equal to 492 Wh/kg.

Another key factor in the charge-discharge test is cycleability, which determines the lifetime of the lithium battery. The discharge capacity decreases with increasing cycles and below 80 % of the initial capacity the end of the lifetime of the battery is reached.

Price, safety, the amount of stored energy, battery life of cycleability, and power output $P=IV$ of a battery is constraints on the commercial application of batteries. The output on discharge of a lithium battery is a current $I=dq/dt$ at a voltage V for a time Δt corresponding to a stored energy:

$$\int_0^{\Delta t} IV(t)dt = \int_0^Q V(q)dq \quad (4.27)$$

where the total charge stored

$$Q = \int_0^{\Delta t} Idt = \int_0^Q dq \quad (4.28)$$

is the battery capacity. For portable batteries, specific energy density (Wh/kg) and volumetric energy density (Wh/cm³) are important factors. The battery life includes not only shelf-life abut also cycle life, defined as number of charge-discharge cycles

before the capacity fades to 80% the initial capacity, $Q/Q_{in.}=0.8$.

4.5 Dielectric Spectroscopy

Dielectric spectroscopy measures the dielectric properties, associated with the conductivity of a sample, as a function of frequency and temperature. It is based on the interaction of an external electric field with the electric dipole moments of the sample. From this data one can obtain the impedance of the solution as a function of frequency. The impedance can then be separated into the frequency dependent conductivity and the relative permittivity of the solution [93].

The dielectric permittivity (ϵ) is directly related to the dimensionless electric susceptibility (χ), which probes how easily a dielectric polarizes in response to an electric field.

$$\epsilon = \epsilon^* \epsilon_0 = (1 + \chi)\epsilon_0 \quad (4.29)$$

where the dielectric constant (ϵ^*) is the relative permittivity of the sample and ϵ_0 is the vacuum permittivity. In dielectric spectroscopy, the sample serves as the dielectric in a parallel-plate capacitor with area (A) and distance (d) between the plates. The dielectric permittivity $\epsilon(\omega)$ is related to the capacitance C (F) as:

$$C(\omega) = \epsilon(\omega) \frac{A}{d} \quad (4.30)$$

The dielectric permittivity is expressed in its real and imaginary components as

$$\epsilon'(\omega) = \epsilon'_\infty + \frac{(\epsilon'_0 - \epsilon'_\infty)}{1 + (\omega\tau)^2} \quad (4.31)$$

$$\epsilon''(\omega) = -i \frac{(\epsilon'_0 - \epsilon'_\infty)\omega\tau}{1 + (\omega\tau)^2} \quad (4.32)$$

where $\omega=2\pi f$ is the angular frequency. When the resistance and the capacitance are present, the resulting combination leads to the classic Debye equation for a single dipole or many dipoles with a single relaxation time.

The starting point in the analysis of dielectric data is

$$\epsilon'' = \frac{(\epsilon_0 - \epsilon_\infty)\omega\tau}{1 + (\omega\tau)^2} + \frac{\sigma}{\omega\epsilon_0} \quad (4.33)$$

The main advantage of this approach is that at some experimental frequency the contribution of dipole loss to the total loss is negligible and hence [93]:

$$\frac{(\epsilon_0 - \epsilon_\infty)\omega\tau}{1 + (\omega\tau)^2} \ll \frac{\sigma}{\omega\epsilon_0} \quad (4.34)$$

With this inequality equation (4.33) becomes:

$$\varepsilon'' = \frac{\sigma}{\omega \varepsilon_0} \quad (4.35)$$

The apparent conductivity (ionic conductivity) can then be calculated from

$$\sigma = \omega \varepsilon_0 \varepsilon'' \quad (4.36)$$

The ionic conductivities of the ionic liquid electrolytes and gel polymer electrolytes were measured as function of temperature by dielectric spectroscopy. The temperature dependence of the conductivity shows the typical non-Arrhenius behavior of liquid electrolytes and is well described by the VTF (Vogel–Tamman–Fulcher) function

$$\sigma = \sigma_0 \exp\left[\frac{-B}{(T - T_0)}\right] \quad (4.37)$$

In the VTF equation, σ_0 is the pre-exponential factor, T_0 is related to the glass transition temperature, and T is the absolute temperature. B is related to the activation energy of ion transport associated with the configurational entropy of the electrolyte [94,95]. Figure 4.13 shows the ionic conductivity and the VTF behavior of a 1M solution of lithium hexafluorophosphate (LiPF_6) in ethylene carbonate (EC)/dimethyl carbonate (DMC) based liquid electrolyte and gel polymer electrolyte.

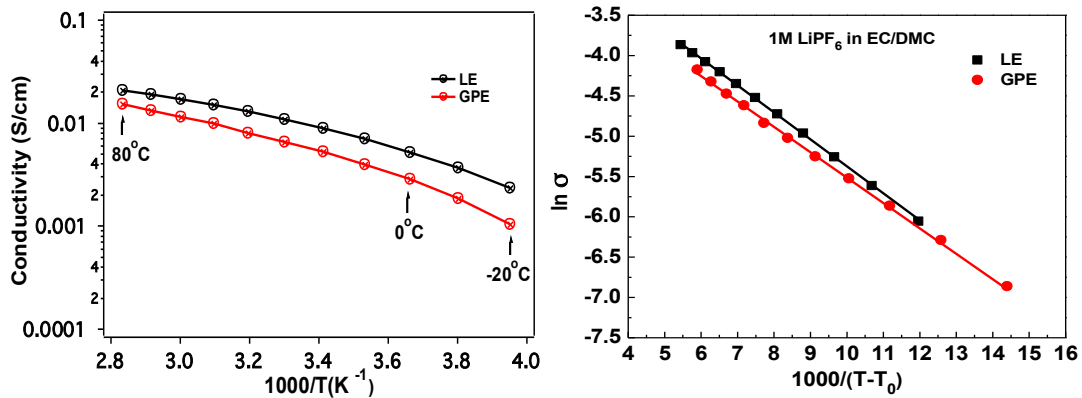


Figure 4.13: Ionic conductivity (left) and VTF behavior (right) of a 1M solution of lithium hexafluorophosphate (LiPF_6) in ethylene carbonate (EC)/dimethyl carbonate (DMC) based liquid electrolyte (LE) and gel polymer electrolyte (GPE).

CHAPTER 5

Summary of Appended Papers

Paper I

A new electrolyte for lithium batteries based on the ionic liquid 1-propyl-3-methyl imidazolium bis(trifluoromethylsulfonyl)imide (PMImTFSI) complexed with {lithium bis(trifluoromethylsulfonyl)imide (LiTFSI)} has been investigated. The new electrolyte shows lower ion coordination than ionic liquid electrolytes based on N-butyl-N-methyl-pyrrolidinium bis(trifluoromethylsulfonyl)imide (Py₁₄TFSI) complexed with LiTFSI and high ionic conductivity at room temperature. An ionic liquid gel electrolyte membrane was obtained by soaking a fibrous membrane, electrospun PVdF-HFP. The ionic liquid-based gel polymer electrolyte exhibited high electrochemical stability and stable cycling performance when assembled with a LiFePO₄ cathode and Li metal anode.

Paper II

A porous LiMnPO₄ cathode material is synthesized by a sol-gel method to increase the power density of rechargeable lithium batteries. The electrochemical performance of the cathode material was evaluated in a cell with an ionic liquid-based polymer electrolyte based on 0.5M {lithium bis(trifluoromethylsulfonyl)imide (LiTFSI)} in 1-ethyl-3-methyl imidazolium bis(trifluoromethylsulfonyl)imide (EMImTFSI). The ionic liquid-based polymer electrolyte shows high ionic conductivity and oxidation stability. Also, the ionic liquid-based polymer electrolyte prevents the dissolution of manganese resulting in a higher cycling stability.

Paper III

A thin flexible polypyrrole-lithium iron phosphate (PPy-LiFePO₄) based cathode has been fabricated. A slurry containing carbon black, a binder and the active material prepared by direct polymerization of pyrrole on the surface of LiFePO₄ (LFP) was spread on an Al/carbon film substrate by the doctor blade method. Transmission electron micrographs reveal that the PPy nanoparticles form a web like structure over the surface of the LFP particles. After doping with lithium ions the PPy network becomes conducting. When evaluated as a cathode of 180 μm thickness together with a gel polymer electrolyte and a lithium anode, the charge-discharge performance reveals that the electrochemical properties of LFP are influenced to a considerable extent by PPy. The cells show high initial discharge capacities of 135 and 110 mAh/g for 0.041 (C/10) and 0.21 (C/2) mA/cm², respectively, and high active material utilization. Furthermore the cell exhibits stable cycle properties even at 0.21 mA/cm² with a low capacity fade per cycle (~ 0.3%).

Paper IV

A new organic cathode material has been prepared from 2,3,6,7,10,11-hexamethoxytriphenylene (HMTP), which is a structure of methoxy functional groups around a triphenylene moiety. The electrochemical redox reaction of HMTP shows high reversibility. A very good cycle performance of a complete cell in the present study also demonstrates the efficiency of the HMTP based cathode. A long time test at OCV shows that HMTP is less prone to self-discharge compared to other organic cathode materials. The reason to this we believe is the delocalization of the free electron over the whole molecule, in contrast to other organic cathode materials containing free radicals, where the charge is localized. Also, HMTP has a crystalline structure preventing the dissolution into the liquid electrolyte, which is otherwise a drawback of several organic electrodes.

Paper V

A nano-fibrous organic radical polymer (PTMA) electrode, fabricated by electrospinning, is proposed as a key component in high performance organic batteries. Cathodes based on PTMA have been proposed before. However, due to an inherent bad electronic conductivity of the radical polymer the electrodes are commonly made with a large amount of carbon black (up to 50%), which in turn limits the energy capacity and the performance of the whole battery. The new strategy with a nano-fibrous morphology allows an extraordinary rate capability, excellent cyclability and at the same time radically decreases the amount of carbon conductor (30%). The nano-fiber organic electrode exhibits stable and large reversible capacities, high columbic and energy efficiencies, and excellent rate capabilities even up to very high charge-discharge rates (50 C). The excellent electrochemical performance is ascribed to the nanostructure that promotes fast ion transport through short diffusion pathways, and at the same time facilitates electron transport.

Paper VI

We propose a solution to overcome the drawback of the organic radical polymer electrode without additional processes for electrode design. Ionic liquid-based polymer electrolyte perfectly prevents the dissolution of the active material into the electrolyte and improves the flexibility of battery. The PTMA organic radical polymer cell composed with N-butyl-N-methylpyrrolidiniumbis(trifluoromethanesulfonyl)imide (Py₁₄TFSI)-based polymer electrolyte does not show any self-discharge. The Py₁₄TFSI-based polymer electrolyte cell show good electrochemical properties despite lower rate capability and cycle stability than liquid electrolyte based analogues due to higher viscosity of Py₁₄TFSI electrolyte.

CHAPTER 6

Conclusions and outlook

1-propyl-3-methylimidazolium bis(trifluoromethylsulfonyl)imide (PMImTFSI)-based polymer electrolytes show high ionic conductivity and high oxidation stability. Moreover, ion coordination is low, and stable cycling performance was observed in cell with a LiFePO_4 cathode.

1-ethyl-3-methylimidazolium bis(trifluoromethylsulfonyl)imide (EMImTFSI)-based polymer electrolyte prevented the Mn dissolution of LiMnPO_4 cathode. Therefore, enhanced cycling stability, increased discharge capacity and longer cycle life was obtained.

The flexible battery, composited with polypyrrol coated LiFePO_4 and gel polymer electrolyte, shows high discharge capacity and excellent cycle life at 0.041 and 0.21 mA/cm^2 even at room temperature.

The new organic cathode material 2,3,6,7,10,11-hexamethoxytriphenylene (HMTP) prevents the self-discharge. Also, the use of single-crystal-structure HMTP prevents dissolution into liquid electrolyte, which is a main drawback of organic electrodes.

The nano-fibrous organic electrode (PTMA) exhibits stable and large reversible capacities, high columbic and energy efficiencies, and excellent rate capabilities even up to very high charge-discharge rates (50C).

An ionic liquid-based polymer electrolyte fully prevents the dissolution of PTMA into the electrolyte and improves the electrochemical stability, self-discharge, and thermal stability. The ionic liquid-based polymer electrolyte composite PTMA battery showed good electrochemical performance.

The market of rechargeable lithium batteries is rapidly growing with development of electronic devices. In recent years, driven by the increased desire for 'green' technologies, the use of rechargeable lithium battery has expanded from portable electronics to large-scale applications, in particular, HEV's and electric vehicles (EVs). There has been recent concern that the amount of the Li resources would not be sufficient to satisfy the increased demands for rechargeable lithium batteries. While there is ample evidence that this is no cause for immediate concern, very large market share of electric vehicles can put a strain on Li production capability. According to a Japanese report published in 2010, about 7.9 million tons of metallic Li will be required when 50% of the oil-driven cars in the world are replaced by XEVs (including hybrid EVs (HEVs) and plug-in HEVs (PHEVs)) [96].

Therefore, new materials are explored in order to replace the lithium-alloyed materials and new battery systems are developed for high power. Novel electrolytes are also essential for increasing high safety of batteries. Flexible battery organic materials have the benefit of high rate capability and low weight. From the new

cathode material and the new type of electrolytes, high safety flexible battery could be assembled. The flexible rechargeable battery will open new market due to convenient fixation.

Acknowledgements

Firstly, I am giving thanks to God who guides me. Four years have passed since I first came to Sweden. Time flies like an arrow! When I came to Sweden, I was an alien and I also felt the culture difference. However, now I love Sweden except Swedish weather.

I am giving grateful thanks to Professor Aleksandar Matic and Professor Per Jacobsson for giving me the opportunity to do a Ph.D here. Professor Per Jacobsson is again specially acknowledged, since he is like a Swedish parent to me. I thank Professor Bruno Scrosati who introduces our group of Chalmers to me.

I am also giving thanks to Ezio Zanghellini and Professor Patrik Johansson for giving advice and help regarding instrument techniques and project work. Annemarie Wagner is acknowledged as a friend to talk to at the beginning, though she did not understand well the meaning of my words. I want to thank Professor Lars Börjesson, Professor Jan Swenson, Professor Maths Karlsson, Bodil Ahlström, Stefano Cazzato, Guo Chen, Young Jin Choi, Maria Grazia Izzo, Maciej Marczewski, Benson Money, Marcel Treskow, Johan Bielecki, Khalid Elamin, Erlendur Jonsson, Susanne Killiches, Jonas Nordström, Jagath Pitawala, Johan Scheers, and Per Sillrén, especially Johan Scheers who is helper for the Swedish life. I am also thankful to Professor Jou-Hyeon Ahn who was my supervisor as a Master student. He collaborates with our group concerning lithium rechargeable batteries and he gives me advice and helps with experimental ideas.

I am giving thanks to my wife who provides the upright way of life and spends her life with me, and daughter and son who teach me parent's way vitalize me and give me unconditional love. I am also giving grateful thanks to be loved my parent and parent-in-law who are eagerly praying for me. I want to be thankful to everybody of Korea and Sweden for their help and prayer.

“I have been with you wherever you have gone, and I have cut off all your enemies from before you. Now! I will make your name great like the name of the greatest man of the earth (from Scripture)”.

Bibliography

- [1] G. Jeong, Y.-U. Kim, H. Kim, Y.-J. Kim, H.-J. Sohn, *Energy Environ. Sci.* 4 (2011) 1986.
- [2] T. Nagura and K. Tazawa, *Prog. Batteries Sol. Cells* 9 (1990) 20.
- [3] J. Hassoun, S. Panero, P. Reale, B. Scrosati, *Adv. Mater.* 21 (2009) 4809.
- [4] K.J. Cho, “The Present Condition of Li-ion Battery Industry in Green Car (in Korean)”, pp. 59-82, Issue of Industry, KDB Research Institute, (2010).
- [5] E. Karden, S. Ploumen, B. Fricke, T. Miller, K. Snyder, *J. Power Sources* 163 (2007) 2.
- [6] D.E. Fenton, J.M. Parker, P.V. Wright, *Polymer* 14 (1973) 589.
- [7] M. Armand, *Solid State Ionics* 9/10 (1983) 745.
- [8] F. Croce, G.B. Appetecchi, L. Persi, B. Scrosati, *Nature* 394 (1998) 456.
- [9] J.M. Tarascon, A.S. Gozdz, C. Schmutz, F. Chmutz, F. Shokoohi, P.C. Warren, *Solid State Ionics* 86-88 (1996) 49.
- [10] M. Walkowiak, A. Zalewska, T. Jesionowski, M. Pokora, *J. Power Sources* 173 (2007) 721.
- [11] X. Li, G. Cheruvally, J.-K. Kim, J.-W. Choi, J.-H. Ahn, K.-W. Kim, H.-J. Ahn, *J. Power Sources* 167 (2007) 491.
- [12] P. Wasserscheid, W. Keim, *Angew. Chem. Int.* 39 (2000) 3772.
- [13] M. Armand, F. Endres, D.R. MacFarlane, H. Ohno, B. Scrosati, *Nat. Mater.* 8 (2009) 621.
- [14] L. Nyholm, G. Nyström, A. Mihranyan, M. Strømme, *Adv. Mater.* 23 (2011) 3751.
- [15] T. Suga, S. Sugita, H. Oshir, K. Oyaizu, H. Nishide. *Adv. Mater.* 23 (2011) 751.
- [16] S.-R. Deng, L.-B. Kong, G.-Q. Hu, T. Wu, D. Li, Y.-H. Zhou, Y. Z.-Y. Li, *Electrochim. Acta* 51 (2006) 2589.
- [17] T. Sarukawa, N. Oyama, *J. Electrochem. Soc.* 157 (2010) F23.
- [18] T. Le Gall, K.H. Reiman, M.C. Grossel, J.R. Owen, *J. Power Sources* 119-121 (2003) 316.
- [19] X. Han, C. Chang, L. Yuan, T. Sun, J. Sun, *Adv. Mater.* 19 (2007) 1616.
- [20] P. Novák, K. Müller, K.S.V. Santhanam, O. Haas, *Chem. Rev.* 97 (1997) 207.
- [21] J.W. Fergus, *J. Power Sources* 195 (2010) 939.
- [22] D. Jugović, D. Uskoković, *J. Power Sources* 190 (2009) 538.
- [23] T. Suga, H. Konishi, H. Nishide, *Chem. Commun.* 17 (2007) 1730.
- [24] J.B. Goodenough, Y. Kim, *J. Power Sources* 196 (2011) 6688.
- [25] B. Xu, D. Qian, Z. Wang, Y. S. Meng, *Mater. Sci. Eng. R* 73 (2012) 51.
- [26] M. Armand et al. U.S Patent No. US7457018B2.
- [27] A.K. Padhi, K.S. Nanjundaswamy, J.B. Goodenough, *J. Electrochem. Soc.* 144 (1997) 1188.
- [28] B. Kang, G. Ceder, *J. Electrochem. Soc.* 157 (2010) A808.
- [29] J. Wolfenstine, J. Read, J.L. Allen, *J. Power Sources* 163 (2007) 1070.
- [30] J.-K. Kim, G. Cheruvally, J.-W. Choi, J.-H. Ahn, D.-S. Choi, C.-E. Song, *J. Electrochem. Soc.* 154 (2007) A839.
- [31] C.K. Jeong, J.H. Jung, B.H. Kim, S.Y. Lee, D.E. Lee, S.H. Jang, K.S. Ryu, J. Joo, *Synthetic Metals* 117 (2001) 99.
- [32] <http://www.nedo.go.jp/roadmap/index.html>.
- [33] P. Delhaes, *Graphite and Precursors*. CRC Press (2001).
- [34] W.-J. Zhang, *J. Power Sources* 196 (2011) 13.

- [35] P. Arora, Z.Zhang, *Chem. Rev.* 104 (2004) 4419.
- [36] Y.M. Lee, J.W. Kim, N.S. Choi, J.A. Lee, W.H. Seol, J.K. Park, *J. Power Sources* 139 (2005) 235.
- [37] G. Venugopal, J. Moore, J. Howard, S. Pandalwar, *J. Power Sources* 77 (1999) 34.
- [38] P.P. Prosini, P. Villano, M. Carewska. *Electrochim Acta* 48 (2002) 227.
- [39] J.W. Fergus, *J. Power Sources* 195 (2010) 4554.
- [40] K. Xu, A. Cresce, *J. Mater. Chem.* 21 (2011) 9849.
- [41] M. Galiński, A. Lewandowski, I. Stepniak, *Electrochim. Acta* 51 (2006) 5567.
- [42] A. Lewandowski, A. Swiderska-Mocek, *J. Power Sources* 194 (2009) 601.
- [43] J.-C. Lassègues, J. Grondin, C. Aupetit, P. Johansson, *J. Phys. Chem. A* 113 (2009) 305.
- [44] P. Hall, G. Davies, J. McIntyre, I. Ward, D. Bannister, K. Le Groeq, *Polym. Commun.* 27 (1986) 98
- [45] D. Payne, P. Wright, *Polymer* 23 (1983) 690.
- [46] H. Xie, X. Tao, J. Guo, *Polymer* 35 (1994) 4914.
- [47] Z. Jiang, B. Carroll, K.M. Abraham, *Electrochim. Acta* 42 (1997) 2667.
- [48] Z. Wang, Z. Tang, *Mater. Chem. Phys.* 82 (2003) 16.
- [49] J.-K. Kim, G. Cheruvally, X. Li, J.-H. Ahn, K.-W. Kim, H.-J. Ahn, *J. Power Sources* 178 (2008) 815.
- [50] F. Croce, R. Curini, A. Martinelli, L. Persi, F. Ronci, B. Scrosati, *J. Phys. Chem. B* 103 (1999) 10632.
- [51] C.M. Yang, H.S. Kim, B.K. Na, K.S. Kum, B.W. Cho, *J. Power Sources* 156 (2006) 574.
- [52] Z. Li, G. Su, X. Wang, D. Gao, *Solid State Ionics* 176 (2005) 1903.
- [53] X. He, Q. Shi, X. Zhou, C. Wan, C. Jiang, *Electrochim. Acta* 51 (2005) 1069.
- [54] G.B. Appetecchi, F. Croce, J. Hassoun, B. Scrosati, M. Salomon, F. Cassel, *J. Power Sources* 114 (2003) 105.
- [55] Y. Liu, J.Y. Lee, L. Hong, *J. Power Sources* 129 (2004) 303.
- [56] J. Doshi, D.H. Reneker, *J. Electrostatics*, 35 (1995) 151.
- [57] S. Cavaliere, S. Subianto, I. Savych, D.J. Jqsones, J. Rozière, *Energy Environ. Sci.* 4 (2011) 4761; <http://www.people.vcu.edu/~glbowlin/electrospinning.htm>.
- [58] S. Ramakrishna, *An introduction to electrospinning and nanofibers*, World Scientific press (2005).
- [59] S.E. Boulfelfel, G. Seifert, S. Leoni, *J. Mater. Chem.* 21 (2011) 16365.
- [60] A.K. Padhi, K.S. Nanjundaswamy, J.B. Goodenough, *J. Electrochem. Soc.* 144(4) (1997) 1188.
- [61] S.Y. Chung, Y.M. Chiang, *Electrochem. Solid State Lett.* 6 (2003) A278.
- [62] P.P. Prosini, M. Lisi, D. Zane, M. Pasquali, *Solid State Ionics* 148 (2002) 45.
- [63] T. Nakamura, Y. Miwa, M. Tabuchi, Y. Yamada, *J. Electrochem. Soc.* 153 (2006) A1108.
- [64] R. Dominko, M. Bele, M. Gaberscek, M. Remskar, D. Hanzel, S. Pejovnik, J. Jamnik, *J. Electrochem. Soc.* 152 (2005) A607.
- [65] M.M. Doeff, Y. Hu, F. McLarnon, R. Kostecki, *Electrochem. Solid State Lett.* 6 (2003) A207.
- [66] J.-K. Kim, G. Cheruvally, J.-W. Choi, J.-U. Kim, J.-H. Ahn, G.-B. Cho, K.-W. Kim, H.-J. Ahn, *J. Power Sources* 166 (2007) 211.
- [67] J.-K. Kim, J.-W. Choi, G. Cheruvally, J.-U. Kim, J.-H. Ahn, G.-B. Cho, K.-W. Kim, H.-J. Ahn, *Mater. Lett.* 61 (2007) 3822.

- [68] P.P. Prosini, D. Zane, M. Pasquali, *Electrochim. Acta* 46 (2001) 3517.
- [69] J.-K. Kim, G. Cheruvally, J.-H. Ahn, *J. Solid State Electrochem.* 12 (2008) 799.
- [70] J.-K. Kim, J.-W. Choi, G.S. Chauhan, J.-H. Ahn, G.-C. Hwang, J.-B. Choi, H.-J. Ahn, *Electrochim. Acta* 53 (2008) 8258.
- [71] J.-K. Kim, G. Cheruvally, J.-H. Ahn, G.-C. Hwang, J.-B. Choi, *J. Phys. Chem. Solids* 69 (2008) 2371.
- [72] K.S. Park, J.T. Son, H.T. Chung, S.J. Kim, C.H. Lee, K.T. Kang, H.G. Kim, *Solid State Commun.* 129 (2004) 311.
- [73] F. Croce, A.D. Epifanio, J. Hassoun, A. Deptula, T. Olczac, B. Scrosati, *Electrochem. Solid State Lett.* 5 (2002) A47.
- [74] J.F. Ni, H.H. Zhou, J.T. Chen, X.X. Zhang, *Mater. Lett.* 59 (2005) 2361.
- [75] H. G. Aurich, *Nitrones, Nitronates and Nitroxides* (eds. S. Patai and Z. Rappoport), p.313, John Wiley & Sons, New York (1989).
- [76] F. MacCorquodale, J. A. Crayston, J. C. Walton, D. J. Worsfold, *Tetrahedron Lett.* 31 (1990) 771.
- [77] T. Katsumata, M. Satoh, J. Wada, M. Shiotsuki, F. Sanda, T. Masuda, *Macromol. Rapid Commun.* 27 (2006) 1206.
- [78] T. Suga, Y. J. Pu, K. Oyaizu, H. Nishide, *Bull. Chem. Soc. Jpn.* 77 (2004) 2203.
- [79] M. Liu, S. J. Visco, L. C. D. Jonghe, *J. Electrochem. Soc.* 137 (1990) 750.
- [80] R. Zniber, R. Achour, M. Z. Cherkaoui, B. Donnio, L. Gehringer, D. Guillon, *J. Mater. Chem.* 12 (2002) 2208.
- [81] D. Bougeard et al. *Infrared and Raman Spectroscopy: methods and applications*, Edited by Bernhard Schrader (VCH Verlagsgesellschaft mbH, Winheim, 1995).
- [82] D.A. Long, *Raman Spectroscopy* (McGraw-Hill, New York, 1977).
- [83] U.P. Agarwal, R. H. Atalla, *Surface analysis of paper*, CRC Press, Inc.: 152-181; (1995).
- [84] J.R. Ferraro, K. Nakamoto, *Introductory Raman Spectroscopy*, Academic Press (1994).
- [85] D.A. Skoog, F.J. Holler, T. Nieman, *Principles of Instrumental Analysis*. New York. pp. 805–808 (1998).
- [86] G. Höhne, W. Hemminger, H.-J. Flammersheim, *Differential Scanning Calorimetry*, published by Springer, (1996).
- [87] X.-Y. Qiu, Q.-C. Zhuang, Q.-Q. Zhang, R. Cao, P.-Zhan, Ying, Y.-H. Qiang, S.-G. Sun, *Phys. Chem. Chem. Phys.* 14 (2012) 2617.
- [88] www.gamry.com
- [89] C.H. Hamann, A. Hamnett, W. Vielstich, *Electrochemistry*, published by Wiley-VCH, (1998).
- [90] J.-K. Kim, J. Manuel, G.S. Chauhan, J.-H. Ahn, H.-S. Ryu, *Electrochim. Acta* 55 (2010) 1366.
- [91] C.M.A. Brett, A.M.O. Brett, *Electroanalysis*, Oxford University Press, (1998).
- [92] D.R. Crow, *Principle and Applications of Electrochemistry*, Blackie, (1994).
- [93] F. Kremer, A. Schonhals, *Broadband Dielectric Spectroscopy*, published by Springer, (2003).
- [94] J.-K. Kim, D.-H. Lim, J. Scheers, J. Pitawala, S. Wilken, P. Johansson, J.-H. Ahn, A. Matic, P. Jacobsson, *J. Korean Electrochem. Soc.* 14 (2011) 92.
- [95] J. Pitawala, J.-K. Kim, P. Jacobsson, V. Koch, F. Croce, A. Matic, *Faraday Discuss.* 154 (2012) 71.
- [96] S.-W. Kim, D.-H. Seo, X. Ma, G. Ceder, K. Kang, *Adv. Energy Mater.* 2 (2012) 710.

